1. Title page

Specific GPCRs Elicit Unique Extracellular Vesicle MiRNA Array Signatures: An Exploratory Study

Xiao Shi, Michelle C. Palumbo, Sheila Benware, Jack Wiedrick, Sheila Markwardt, Aaron Janowsky

Affiliations:

XS, SB, AJ: Research Service, Veterans Affairs Portland Health Care System, Portland OR 97239

MCP, AJ: Department of Behavioral Neuroscience, Oregon Health & Science University, Portland OR 97239 USA

JW, SM: Biostatistics & Design Program, OHSU-PSU School of Public Health, Oregon Health & Science University, Portland OR 97239 USA

AJ: Department of Psychiatry, Oregon Health & Science University, Portland OR 97239 USA

Laboratory of Origin:

Aaron Janowsky, Research Service, Veterans Affairs Portland Health Care System

Oregon Health & Science University, Portland OR 97239 USA

2. Running title page

Running title: Activating GPCRs regulates extracellular vesicle miRNA content

Corresponding author: Xiao Shi, Ph.D.

Address: Research Service, VA Portland Health Care System, 3710 SW US Veterans Hospital Rd., Portland, OR 97239

Telephone: (503) 418-5376

Fax: (503) 721-7839

Email: shixi@ohsu.edu

Number of text page: 36

Number of tables: 1

Number of figures: 4

Number of references: 105

Abstract word count: 225

Introduction word count: 672

Discussion word count: 1779

Nonstandard abbreviations used: ACKR3, atypical chemokine receptor 3; ADORA1, adenosine receptor A1; ANOVA, analysis of variance; CCPA: 2-Chloro-N^6-cyclopentyladenosine; DPCPX, 8-Cyclopentyl-1,3-dipropylxanthine; ERK, extracellular signal-regulated kinase; EV, extracellular vesicle; FZD4, frizzled class receptor 4; GPCR, G protein-coupled receptor; HRH1, histamine receptor H1;

40 KEGG, Kyoto Encyclopedia of Genes and Genomes; miRNA, microRNA; NTA, nanoparticle tracking
41 analysis; PEA, 2-pyridylethylamine; PPI, protein-protein interaction; qPCR, quantitative polymerase
42 chain reaction; SEC, size exclusion chromatography; SDF-1α, stromal derived factor-1α; TEM,
43 transmission electron microscopy; Wnt3A, Wnt family member 3A.

3. Abstract:

All cells secrete extracellular vesicles (EVs) containing nucleic acid cargo, including microRNAs (miRNAs), that regulate the function of receiving cells. G protein-coupled receptors (GPCRs) affect intracellular function via multiple signaling cascades. However, the mechanisms of GPCR intercellular signaling through EV miRNA activity are unknown. Human U2 osteosarcoma cells expressing native GPCRs were used to selectively stimulate distinct G protein signaling cascades ($G\alpha_i$, $G\alpha_q$, $G\alpha_{12/13}$, and β-arrestin) by members of specific receptor subclasses including the adenosine receptor A1 (ADORA1), the histamine receptor H1 (HRH1), the frizzled class receptor 4 (FZD4), and the atypical chemokine receptor 3 (ACKR3), respectively. We hypothesized that stimulation of specific classes of GPCRs would cause the release of EVs containing miRNAs with receptor-specific up- or down-regulated expression, affecting unique pathological downstream signaling cascades. Receptor-specific agonists dose-dependently increased respective signaling cascade intermediates. We found no change in the quantity of EVs (~200nm diameter), but there were distinct EV miRNA signatures following stimulation of GPCRs. Network analyses of differentially expressed miRNA and their predicted targets validated the linkage between specific receptors and cell function and pathological states. The data can be used to reverse engineer mechanisms involving EV miRNAs for various physiological and pathological processes. GPCRs are major pharmacological targets, so understanding the mechanisms that stimulate or inhibit GPCR-mediated changes in extracellular miRNA signatures could improve long- and short-term therapeutic and unwanted drug effects.

Summary: Stimulation of specific GPCRs elicited unique EV miRNA signatures that up- and down-regulated predicted biological and pathological cellular processes.

Key words

G protein-coupled receptor, receptor signaling, miRNA, extracellular vesicle, U2OS

4. Significance Statement

G protein-coupled receptors (GPCR) are therapeutic targets for various human diseases. However, the mechanisms of GPCR signaling through extracellular vesicle (EV) miRNA activity are unknown. Here, we identified unique EV miRNA signatures resulting from GPCR activation. The miRNA functional analyses indicate that the downstream signaling effects and their functional networks differ by receptor. This study has important implications for developing new drugs and their long-term and "off-target" effects.

5. Visual Abstract

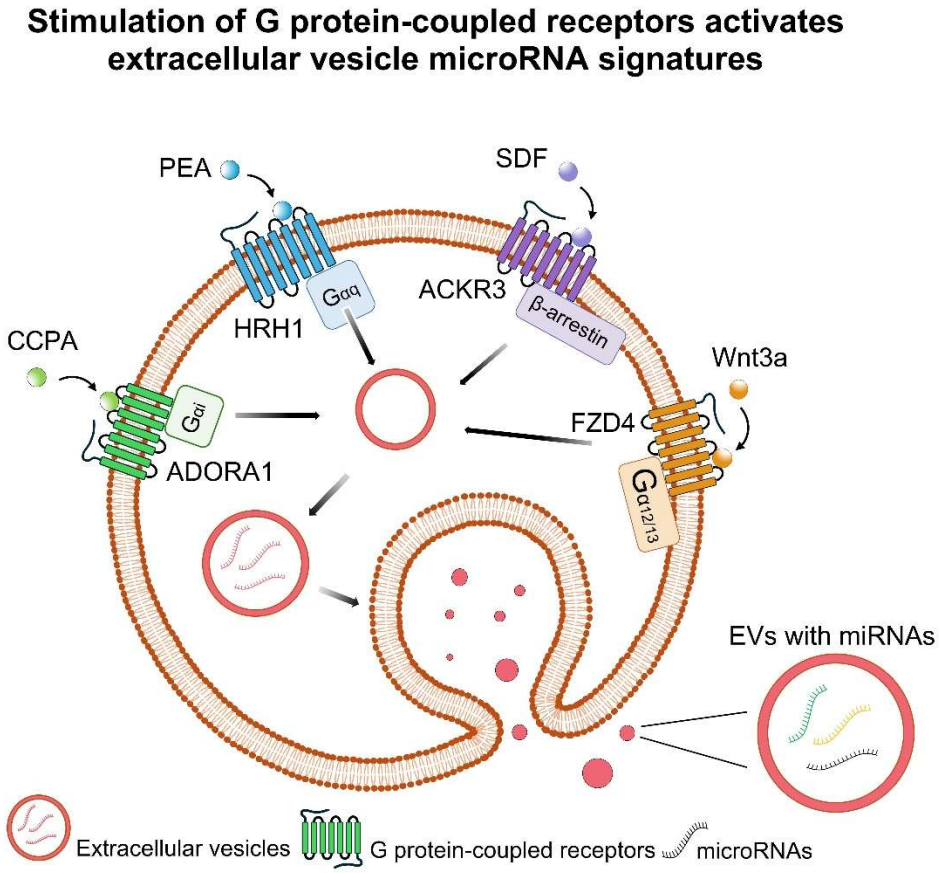

6. INTRODUCTION

G protein-coupled receptors (GPCRs) comprise a protein superfamily with five major branches: glutamate, rhodopsin, adhesion, frizzled/taste 2, and secretin (Stevens et al., 2013). These transmembrane proteins transduce neurotransmitter signals from outside the cell to affect internal cellular function (Stevens et al., 2013). Translation of extracellular signals to intracellular biochemical cascades is a multistep process involving specific receptor-ligand interactions, conformational changes allowing interactions with regulatory G proteins such as, $G\alpha_i$, $G\alpha_q$, $G\alpha_{12/13}$, and β-arrestin, and activation of specific effector systems (Asher et al., 2022; Heydenreich et al., 2023). GPCR function or malfunction is implicated in numerous human diseases, and approximately 700 medications are designed to target GPCRs and related proteins (Sriram & Insel, 2018) and to alter cellular activity. In addition to the canonical intracellular protein cascades, GPCR signaling is both a precursor and effector of extracellular mechanisms of communication (Bebelman et al., 2020).

Cells interact through the secretion and uptake of extracellular vesicles (EVs) (Rothman, 1996). EVs are a heterogeneous population of membrane vesicles that are classified into exosomes, microvesicles, and apoptotic bodies based on their biogenesis, release pathways, size, content, and function (Doyle & Wang, 2019; Palmisano et al., 2012). EVs transport a range of molecules such as nucleic acids including microRNAs (miRNA), lipids, and proteins associated with the cell lipid membrane such as GPCRs (Kahn et al., 2017; Mack et al., 2000). GPCRs and EVs have interacting functions since EV biogenesis and release can be regulated by GPCR stimulation, and EVs can contribute to GPCR signaling (Kriebel et al., 2018; Frederik Johannes Verweij et al., 2018). In fact, a number of GPCRs alter EV release and/or EV cargo (Bhattacharya et al., 2023; Conrad et al., 2020; Lee et al., 2023). However, the effects of stimulating specific GPCR subclasses, in head-to-head comparisons, on EV content and subsequent alteration of receiving cell function remain to be elucidated (Tetta et al., 2013).

MiRNAs are small non-coding RNAs (Tabara et al., 2002) and play crucial roles in plant and animal physiology, including development (Zhang et al., 2015). They are implicated in symptoms of pathology at the intersection of substance use and HIV (Odegaard et al., 2020), Alzheimer's disease (Sandau et al., 2022), and diabetes (Chao et al., 2023). MiRNAs function by translationally repressing target mRNA transcripts. The human genome includes approximately 2,600 miRNAs, and individual miRNAs can regulate tens to hundreds of gene targets (Plotnikova et al., 2019). Therefore, miRNAs are one of the largest classes of regulatory RNAs that affect complex genetic networks. However, whether GPCRs are post-transcriptionally affected by miRNAs is controversial (Ofer & Linial, 2022; Orr-Burks et al., 2021).

Many drugs that stimulate GPCRs affect EV miRNA disposition. For example, ethanol potentiates GABA-A receptor function and alters EV miRNA expression (Bourgeois et al., 2023). Methamphetamine use alters groups of human plasma EV miRNAs (Sandau et al., 2020). Bombesin receptor subtype 3 stimulation results in its own incorporation into EVs and alteration of RhoA function in receiving cells (Z. Wang et al., 2022). GPCRs affect EV secretion and miRNA expression pertaining to platelet aggregation, function, and activation (Ambrose et al., 2018; Jin et al., 2022). Additionally, stimulation of CXCR7, a chemokine receptor, results in expression changes of specific miRNAs related to colorectal cancer metastasis. However, it is unknown if stimulation of specific GPCR subclasses affects EV miRNA content to alter downstream cellular communication, as well as signal cascades involved in physiology and disease. Using U2OS cells, we examined the effects of stimulating the adenosine receptor A1 (ADORA1), the histamine receptor H1 (HRH1), and atypical chemokine receptor 3 (ACKR3), members of the Rhodopsin-like GPCR family, as well as the frizzled class receptor 4 (FZD4). These receptors are $G\alpha_i$-, $G\alpha_q$-, β-arrestin-, and $G\alpha_{12/13}$-coupled, respectively. Stimulation resulted in the release of EVs with unique miRNA signatures. Network analyses of EV miRNA target transcripts showed both up- and down-regulation of protein cascades involved in physiological and pathological states of cell function. This

work demonstrates the large-scale genetic influence of miRNA arrays as a product of GPCR stimulation and can be used to characterize down-stream pharmacological effects of receptor-drug interactions.

7. RESULTS

GPCR expression in U2OS cells

To characterize the effect of GPCR stimulation on EV miRNA content, we examined GPCR expression in different cell lines from The Human Protein Atlas (Karlsson et al., 2021). We determined that the human osteosarcoma cell line, U2OS, likely expressed receptors from multiple branches of the GPCR family tree (https://www.proteinatlas.org/search/U2OS+cells), including rhodopsin, adhesion, and frizzle/taste receptors, each associated with differing G-protein cascade activation (Supplemental Tab. S1). Numerous other cell lines including U-251MG, A-431 and SH-SY5Y, were considered but not used because they did not highly express a significant spread of receptor subtypes (Supplemental Tab. S1). Additionally, we avoided the use of transfected or over-expressing cells because the transfection and selection protocols could have their own effects on EV synthesis, expression, and cargo selection (Im et al., 2019; Németh et al., 2017; Nordin, 2022). The protein expression data of U2OS cells provided by the Human Protein Atlas database indicated that ADORA1, HRH1, ACKR3, and FZD4 were expressed at levels sufficient to demonstrate second messenger system activity, i.e., function.

The expression of these receptors in U2OS cells was further validated through various functional assays. 2-Chloro-N^6-cyclopentyladenosine (CCPA), an ADORA1 selective agonist, dose-dependently inhibited forskolin-induced cAMP levels (Fig. 1A). The inhibition of cAMP by CCPA was reduced by antagonist 8-Cyclopentyl-1,3-dipropylxanthine (DPCPX), suggesting that the decreased cAMP level resulted from ADORA1 activation. The activation of HRH1 was assessed by measuring inositol monophosphate (IP1) accumulation following 2-pyridylethylamine dihydrochloride (PEA) stimulation, and the effect was

abolished by the HRH1 antagonist cetirizine (Fig. 1B). To evaluate the function of FZD4, we measured the activity of alkaline phosphatase (ALP), the downstream gene product of the Wnt/β-catenin signaling cascade. Norrin, another FZD4 agonist, has high affinity (Xu et al., 2004). However, Norrin is difficult to purify from mammalian sources (Perez-Vilar & Hill, 1997). We found the commercially available Norrin (R&D Systems) did not stimulate FZD4 (data not shown). Although Wnt family member 3A (Wnt3A) can bind to several members of the frizzled receptor family, it has much higher affinity binding at FZD4 than FZD8 (Kozielewicz et al., 2021), and both are expressed in U2OS cells. Therefore, we used Wnt3A as the FZD4 ligand. Wnt3A significantly increased ALP activity compared to the vehicle control (VC) (Fig. 1C). The endogenous chemokine ligand stromal derived factor-1α (SDF-1α) induced ERK1/2 phosphorylation through chemokine receptor, ACKR3 (Fig. 1D). Phospho-ERK1/2 levels were normalized to total ERK1/2 as shown on the immunoblot (Supplemental Fig. S2). Thus, we selected a dose of 10μM of CCPA, 200μM of PEA, 100ng/ml of Wnt3A and SDF-1α to selectively stimulate ADORA1, HRH1, FZD4, and ACKR3, respectively.

EV characterization from U2OS cells

First, we evaluated native U2OS EVs isolated from the culture media using ultrafiltration followed by size exclusion chromatography (SEC). The immunoblot revealed the presence of EV surface markers, tetraspanins CD9, CD63, and CD81 (Fig. 2A), in SEC fractions 7, 8, and 9. We also detected EV cytosolic markers syntenin (Kugeratski et al., 2021) and flotillin-1 in individual fractions 7-9. In addition, calnexin, an endoplasmic reticulum marker and a negative EV control, was absent in fractions 7-9 (Fig. 2A). All EV markers were absent in the media control sample, which suggested that the SEC fractions 7-9 were enriched in EVs from U2OS cells. The pooled EV-enriched fractions 7-9 were assessed for vesicle shape and size by TEM, which revealed vesicular structures ranging from 100-200 nm (Fig. 2B, red arrows). We quantified the EV concentration and size distributions using fluorescence nanoparticle tracking analysis (f-NTA), which enhances the detection of membrane vesicles by incorporation of a

fluorophore into the EV lipid membrane. The average concentration of EVs in U2OS culture supernatant was $6x10^9$ particles/mL (Fig. 2C, D), which was significantly increased compared to the media control. Despite using EV-depleted FBS, some residual bovine EVs, especially small-size EVs (Pham et al., 2021), remained in the media control, with an average concentration of $4.45x10^9$ particles/mL (Fig. 2C, D). However, they did not exhibit the EV markers we examined (Fig. 2A). Thus, those vesicles are most likely not derived from the host cell (Lehrich et al., 2021). Therefore, media control samples were included in all subsequent experiments to avoid any miRNA artifacts caused by serum. The size of EVs ranged from 50-500 nm with no significant difference in the median diameter between the media control (214 ±14.41nm) and U2OS-exposed media (237± 5.17 nm) (Fig. 2C). We also compared the EV concentration in various GPCR agonist treatment groups with their vehicle controls. Notably, the EVs from agonist-treated samples and vehicle controls exhibited similar concentration and size, with median diameter ranging from 210-240nm (Supplemental Fig. S3). Therefore, the pooled EV-enriched SEC fractions 7-9 were used for further miRNA assessment.

EV miRNAs differentially expressed following GPCR stimulation

We utilized high-throughput miRNA arrays to identify EV miRNA signatures following receptor activation. To analyze the EV miRNAs from stimulated receptors and avoid any confusion posed by the miRNA content in the media from non-stimulated cells, we excluded any miRNAs that were only present in the media control (Supplemental Table. S2) or were changed less than 10-fold (< 3.3 PCR cycles) between the media control and vehicle control. This allowed us to focus on analyzing specific receptor stimulation effects. We identified 105 miRNAs associated with ADORA1, 92 with HRH1, 88 with FZD4, and 86 with ACKR3 that expressed in at least 80% of either vehicle control or the agonist-treated samples and underwent statistical analysis. To further narrow down our miRNA of interest after receptor stimulation, we performed differential-expression testing using within-pairs linear regression and calculated *p*-values using a nonparametric rank-based (Skillings-Mack) test. This approach provided unbiased estimates of stimulation-treatment effects. We subsequently ranked the miRNAs within each

receptor type by magnitude of effect and selected all miRNAs with Skillings-Mack p-value < 0.2 for further investigation, emphasizing discovery power over avoidance of false positive results. Any miRNAs with absolute fold change ≥ 1.5 ($|\Delta\Delta Cq| \geq 0.585$) were chosen for enrichment analyses.

We directly compared the miRNAs expression across each receptor. The heat map illustrated distinct EV miRNA patterns unique to each receptor (Fig. 3A). Our analysis showed that 29 miRNAs were differentially expressed in the ADORA1 group compared to its vehicle control, with 10 miRNAs demonstrating an absolute fold change greater than 1.5 (Fig. 3B). Furthermore, 5 out of 10 miRNAs were observed with $p < 0.05$ (Table 1). For the HRH1 group, 3 out of 4 differentially expressed miRNAs were found to have $p < 0.05$ (Fig. 3C and Table 1). In contrast, among the 22 differentially expressed miRNA in FZD4 group, 10 exhibited an absolute fold change greater than 1.5 (Fig. 3D), but only one miRNA (miR-203a-3p) met the threshold of $p < 0.05$ (Table 1). A similar pattern was also observed in the ACKR3 group (Fig. 3E and Table 1). Additionally, we further assessed the shared and non-shared changes in miRNAs with at least 1.5-fold change in either direction for each receptor (Fig. 3F). We found that miR-550a-5p, miR-502-3p, miR-137, and miR-422a were the most changed miRNAs following ADORA1, HRH1, FZD4, and ACKR3 stimulation, respectively (refer to Supplemental Table S3 for a complete list of all differentially expressed miRNAs of individual receptors and raw data in data availability section).

MiRNA targets and pathway predictions following GPCR stimulation

We next performed target prediction and functional annotations on all miRNAs of interest that exhibited an absolute fold-change ≥ 1.5 (Fig. 3) for each receptor. For analysis involving multiple miRNAs, we selected gene targets predicted by at least two miRNAs for functional analysis through the Kyoto Encyclopedia of Genes and Genomes (KEGG) database. Following ADORA1 stimulation, we identified 3,562 miRNA predicted target genes, with 709 predicted genes targeted by at least two differentially regulated miRNAs. The top 25 enriched KEGG pathways associated with ADORA1 miRNA targets are

primarily related to cell proliferation, apoptosis, and cancer (Fig. 4A). After HRH1 stimulation, 357 predicted miRNA targets were selected for enrichment analysis. Many of the top predicted miRNA target enriched KEGG pathways were linked to various cancers (Fig. 4B). We observed significant enrichment of FoxO and ErbB signaling (Fig. 4B), which play crucial roles in angiogenesis, cell proliferation, apoptosis, and modulation of the immune response (Appert-Collin et al., 2015; Kim et al., 2022; Lam et al., 2013; Ryzhov et al., 2017), and are associated with HRH1 function (Fernández-Nogueira et al., 2018; Hatipoglu et al., 2023; Li et al., 2022). Additionally, we found that HRH1 miRNA predicted targets are enriched in endocrine and nervous system pathways. For instance, several hub genes identified in HRH1 miRNA target PPI network, such as PTEN, MYC, GSK3B, and SMAD3 (Supplemental Fig. S4), are known to be involved in insulin signaling (Cheung et al., 2010; Li et al., 2020; Patel et al., 2008; H. L. Wang et al., 2022). The most upregulated miRNA from HRH1 stimulation, miR-502-3p, was associated with multiple enriched pathways related to insulin resistance, including EGFR tyrosine kinase inhibitor resistance, AGE-RAGE signaling pathway in diabetic complications, and pancreatic cancer (Supplemental Fig. S5A). Overall, these findings suggest that altered miRNA expression following HRH1 activation may play a role in diabetes.

Generally, the miRNA targets of FZD4 were related to cancer, drug resistance, embryonic development, and aging (Fig. 4C). The most downregulated miRNA after FZD4 stimulation, miR-137, had targets that are enriched in GABAergic and dopaminergic synapses, suggesting its role in the regulation of synaptic function (Supplemental Fig. S5B). Additionally, miR-137 targets were linked to substance abuse and neurogenerative disease (Supplemental Fig. S5B). MiR-135b-3p and miR-422a exhibited increased expression following FZD4 and ACKR3 activation (Fig. 3D, 3E, and Supplemental Table S3). Therefore, some of the enriched pathways, including various cancer types and signaling pathways, shared similarities between two receptors (Fig. 4C and Fig. 4D). Alongside cancer-related pathways, several enriched pathways related to aging and neurodegenerative diseases, such as cellular senescence and autophagy were identified as ACKR3 miRNA targets (Fig. 4D). Insulin resistance-related pathways were also

observed when analyzing miRNA targets following ACKR3 stimulation (Fig. 4E). Note, however, that the top identified hub genes between the two receptors were distinct (Supplemental Fig. S4), suggesting FZD4 and ACKR3 may regulate the same cellular process through different mechanisms.

8. DISCUSSION

We hypothesized that stimulation of GPCRs can regulate the EV miRNA profile. We used a combined approach of ultrafiltration and SEC to isolate EVs from agonist-stimulated culture media, then followed up with miRNA qPCR arrays. Our findings provide evidence that within a single cell type, head-to-head comparisons of specific agonist-stimulation of GPCR subclasses reveal unique EV miRNA profiles.

Although various methods exist for isolating EVs, obtaining a high yield of pure EVs with minimal contamination is challenging (Sidhom et al., 2020). Combining ultrafiltration with SEC allowed us to isolate EVs with sufficient yield and purity, and that are suitable for further EV miRNA characterization. We noticed the median size of EVs measured by NTA was larger than the size reported by TEM. While f-NTA was utilized in this study to enhance membrane vesicle detection, it may not differentiate EVs from other similar particles, such as protein aggregates and lipoproteins. This overlap could lead to overestimating the EV size and impacting the accuracy of EV detection. Furthermore, this discrepancy could be due to EV storage and freeze-thaw cycles (Gelibter et al., 2022; Görgens et al., 2022). In contrast to freshly prepared samples for TEM, EV aggregation after the freeze-thaw cycle could result in increased particle size detected by NTA. Contrary to other studies that have reported increased EV release after GPCR stimulation (Ambrose et al., 2018; Conrad et al., 2020), we did not find significant changes in either the quantity or mean diameter between vehicle control and agonist-treated samples. We postulate that our EV production results could be due to the cell type and culture conditions (Bost et al., 2022; Palviainen et al., 2019). In addition, serum vesicles are a major source of EV contamination from the cell culture media. To minimize serum-derived EVs, our cells were cultured with EV-depleted FBS, which

may have a reduced ability to support cell growth (Bost et al., 2022). Therefore, different isolation methods and cell culture conditions could result in variations in EV concentrations.

Few studies have addressed GPCR activation and its stimulation of EV release in cultured cells (Alonso et al., 2011; Conrad et al., 2020; Mazzeo et al., 2016; F. J. Verweij et al., 2018), and indicating that GPCR signaling can regulate EV biogenesis and release. For instance, activation of (only) muscarinic receptor type I induces multivesicular body formation and stimulates EV secretion in T lymphocytes (Alonso et al., 2011). Similarly, stimulating (only) HRH1 promotes the exocytosis of multivesicular bodies in HeLa cells (Frederik Johannes Verweij et al., 2018). Conrad et al. demonstrated that activation of multiple endogenous GPCRs stimulates EV release from trophoblasts (Conrad et al., 2020). Moreover, numerous studies have shown that the activation of GPCRs regulates the expression of individual miRNAs. For example, activation of the estrogen receptor inhibits miR-148a levels in breast cancer cells and COX-2 induces miR-526b expression through the prostaglandin receptor, which promotes breast cancer progression (Majumder et al., 2015; Tao et al., 2015). However, the aforementioned studies did not investigate EV miRNA expression after GPCR stimulation. Ambrose et al. identified released miRNA patterns that are highly correlated with specific GPCR agonists in platelets (Ambrose et al., 2018). However, their miRNA analysis used EV-rich supernatant after GPCR stimulation, which included both non-EV and EV miRNAs. Here, we focused on EV miRNA profiles following GPCR stimulation. We found many of the EV miRNAs were similar across the four GPCR subgroups, although some unique miRNAs were associated with each receptor. We identified 10 miRNAs in ADORA1, 4 miRNAs in HRH1, 10 miRNAs in FZD4, and 6 miRNAs in ACKR3 that were differentially expressed following agonist stimulation. We found that a greater number of miRNAs showed increased expression levels compared to those with decreased expression after receptor activation. The increase in miRNAs ranged from 6 to 30% more than decreased miRNAs, depending on the specific receptor group. For example, following ADORA1 activation, there were about 15% more increased than decreased miRNAs, while in

the FZD4 group, there was a 6.3% higher number of increased miRNAs. Additionally, we observed a few miRNAs that exhibited more than a 1.5-fold change after each receptor activation. While endogenous miRNAs may be present in lower amounts in EVs, their functional significance can be considerable. Brown et al. demonstrated that a threshold concentration of miRNA is necessary to suppress target genes (Brown et al., 2007). This suggests that EV miRNAs may play a crucial role in miRNA expression in the recipient cells, helping them reach the required threshold to elicit specific effects.

Our study directly compared the stimulation of specific GPCR subclasses and the unique EV miRNA signatures that might dictate downstream $G\alpha_i$, $G\alpha_q$, $G\alpha_{12/13}$, and β-arrestin protein cascades. G proteins transduce the extracellular signals to the appropriate downstream effectors. Multiple GPCRs can couple to the same type of G protein. One GPCR also can interact with different G proteins to trigger multiple pathways. Previous reports showed that overexpression of Gα12 can alter multiple miRNA levels (Yang et al., 2015), suggesting that G proteins may play a role in controlling miRNA expression after GPCR stimulation. Despite our result suggesting a unique miRNA signature for each receptor, it is not clear that a miRNA signature was associated with specific types of G proteins due to the limited sample size (four receptors). Future studies are necessary to resolve whether EV miRNAs are regulated by specific G proteins after GPCR stimulation.

The mechanisms by which miRNAs are sorted into EVs are not fully understood. However, several RNA-binding proteins and membrane-associated proteins have been identified that could influence this sorting process (Martins-Marques et al., 2022; Villarroya-Beltri et al., 2013; Yoon et al., 2015). Argonaute 2 (Ago2), a core component of the RNA-induced silencing complexes, binds to miRNAs and facilitates their sorting. Ago2 can be regulated by the various cellular signaling pathways (Horman et al., 2013; Jackson et al., 2022; McKenzie et al., 2016). For instance, McKenzie *et al.* demonstrated that KRAS-dependent activation of MEK-ERK can phosphorylate the Ago2 protein, thereby facilitating the sorting of specific miRNAs into EVs (McKenzie et al., 2016). In differentiated PC12 cells, the activation of Gαq

leads to the formation of Ago2-associated granules, which selectively sequester unique transcripts (Jackson et al., 2022). Another important molecular mediator is Connexin 43, which directly binds to specific miRNAs and sorts them into EVs (Martins-Marques et al., 2022). ACKR3, one of the GPCRs we studied here, when activated by an agonist, inhibits the function of Connexin 43 (Fumagalli et al., 2020). Furthermore, ADORA1 can directly interact with the membrane protein Caveolin 1, which has an established role in EV cargo selection (Ginés et al., 2001; Lee et al., 2019). Currently, there is no consistent mechanism for miRNAs sorting into EVs across different cell types. However, GPCRs and downstream signaling can directly or indirectly interact with those proteins involved in the sorting process, which could employ distinct mechanisms to influence the EV miRNA content. Future studies exploring the role of GPCRs, G proteins, and GPCR signaling in the expression, localization, activity, and post-translational modification of molecular mediators, such as Ago2 and Connexin 43, could provide valuable insights into how GPCRs regulate specific miRNAs within EVs and potentially lead to therapeutic applications.

When we compared the predicted functional effects of EV miRNAs across the four GPCRs, we found that numerous enriched pathways were associated with human cancers. For instance, the targets of HRH1 miRNA were enriched in colorectal cancer, breast cancer, and melanoma, which were consistent with previous findings (Li et al., 2022; C. Park et al., 2023; Shi et al., 2019). This could be because many of the predicted miRNA targets that are involved in a wide range of cellular activities, such as cell proliferation, differentiation, migration, and apoptosis, that contribute to cancer initiation, progression and metastasis (Evan & Vousden, 2001; Matthews et al., 2022; Pfeffer & Singh, 2018). Additionally, the top hub genes identified in the PPI network of FZD4 miRNA targets, including MYC, EGFR, MDM2, and CDK1 (Supplemental Fig. S4), were also involved in many aspects of cancer progression (Gabay et al., 2014; Oliner et al., 2016; Sigismund et al., 2018; Wang et al., 2023). This finding may contribute to

understanding the mechanism of GPCR activities in cancer progression and to the development of new pharmacotherapies.

Moreover, our data revealed functional differences among the four GPCRs. When we compared the differentially expressed miRNAs and their predicted pathways across four GPCRs, we found ADORA1 had a unique set of miRNAs that did not overlap with the other 3 GPCRs. Three significantly altered ADORA1 miRNAs, miR-135a-5p, miR-31-5p, and miR-454-3p, are associated with cardioprotection (Chen et al., 2022; Liu et al., 2024; Wang et al., 2021; Zhao et al., 2024), supporting the established role of ADORA1 in the protection of cardiomyocytes during ischemia (Crawford et al., 2005; Reichelt et al., 2005). We observed that several insulin-resistant pathways were enriched among the targets of HRH1 miRNAs. The two significantly elevated HRH1 miRNAs, miR-502-3p and miR-423-5p, affect glucose metabolism (Liu et al., 2023; Montastier et al., 2019; Yang et al., 2017). Notably, miR-423-5p has been identified as a potential biomarker of severe obesity (Ortega et al., 2013). Consistent with previous studies (Shi et al., 2019; Wang et al., 2010), our findings indicate that HRH1 may play a role in regulating insulin sensitivity. MiR-137 and miR-518e-3p were solely expressed in EVs from cells treated with FZD4 agonist, and not after activation of other receptors, suggesting they may serve as unique signatures of FZD4 activation. Interestingly, genome-wide association and proteomic studies have implicated the *MIR137* host gene, and the mRNA targets of miR-137 are risk genes for schizophrenia (Palumbo et al., 2023; Ripke et al., 2014). Although the FZDs activation mechanism and FZDs-G protein interaction are still not fully understood (Arthofer et al., 2016; Strakova et al., 2017; Zhang et al., 2024), this study could lead to the identification of new miRNA targets for GPCR activation and post-transcriptional mRNA gene targets as a down-stream effector for rational drug design. The predicted pathways for ACKR3 miRNA indicated that 9 of the top 25 significantly enriched pathways were associated with aging and neurodegenerative diseases. Cell senescence, which is a permanent cell growth arrest and linked to aging and several neurodegenerative disorders (Kritsilis et al., 2018; Papadopoulos et al., 2020; Suelves et al.,

2023), was observed with the highest gene count among those pathways. Additionally, miR-135b, the only significantly increased ACKR3 miRNA, promotes hippocampal cell proliferation and enhances learning and memory by affecting the rate-limiting enzyme for β-amyloid production. miR-135b is significantly reduced in the peripheral blood of Alzheimer's disease patients (Zhang et al., 2016). GPCRs play a significant role in various diseases through different mechanisms of action. Our study suggests that the alteration of specific miRNA expression following GPCR activation by pharmacotherapies may introduce a new mechanism through which GPCRs regulate extracellular events by modulating the expression of miRNAs in EVs.

This study highlights the novel mechanism of EV miRNA content regulated by GPCRs. However, there are limitations in the current study. The EVs used for miRNA analysis are a heterogeneous population, of various but similar sizes, and may originate from different biogenesis pathways and exhibit distinct biological functions. GPCR agonists (or vehicles) may stimulate production of different subclasses of the EVs, such as exomeres, exosomes, or even microvesicles, and affect their content. Further experiments with optimized isolation methods are needed to investigate changes in EV subpopulations and miRNAs regulated by GPCRs. U2OS cells expressing endogenous GPCRs were used as a model to explore EV miRNA profiles. Thus, the differentially expressed miRNAs detected in the current study could be cell-type specific. EV content and miRNA expression could vary by cell type and culture conditions. Further research should investigate EV miRNA expression changes after receptor stimulation across different cell lines, particularly those related to diseases. For example, MDA-MB-231 is a breast cancer cell line that expresses several GPCRs, including adenosine, histamine, adhesion and chemokine receptors (Panjehpour et al., 2005; Chulo Park et al., 2023; Sarmoko et al., 2025). Utilizing this cell line could provide valuable insights into the EV miRNA pattern associated with breast cancer in response to GPCR stimulation.

In this exploratory study, we used bioinformatics to predict the target genes and enriched pathways of the differentially expressed miRNAs following GPCR activation. While computational analyses can effectively identify potential miRNA targets, future research needs to focus on validating these

candidates. For instance, the pathways enriched for miR-137, the most decreased miRNA following frizzled receptor activation, were found to be involved in GABAergic synapses, dopaminergic synapses, long-term potentiation, and autophagy (Supplemental Fig. S5B). These enriched pathways are essential for nerve activity and synaptic plasticity, which is consistent with the crucial role of FZD4 in brain development (Zhang et al., 2017; Zhang et al., 2023). Notably, an independent study from our laboratory confirmed that the delivery of miR-137 regulates synaptic proteins in both neuronal cell cultures and the mouse frontal cortex (Palumbo et al., 2023), which demonstrates the biological effect of miR-137 and its gene targets, aligning with our pathway prediction. Our study might illustrate a potential pathway for miRNAs and their targets in response to various stimuli. Future directions should aim to validate the top differentially expressed miRNAs identified after each GPCR activation and assess their gene targets in cellular contexts. Additionally, using proteomics to evaluate the molecular changes in an *in vivo* model following miRNA delivery will help enhance our understanding of the underlying mechanisms and explore the functional implications for clinical relevance.

In summary, we characterized EV miRNA profiles from U2OS cells after stimulation of specific GPCR subclasses with selective agonists. We identified unique EV miRNA signatures resulting from GPCR subtype activation. The functional analyses revealed that the predicted gene targets of the EV miRNAs were enriched in distinct metabolic pathways, including physiological and pathological states of cell function. This study offers a novel biological mechanism, EV miRNA content regulation by stimulated GPCRs, and provides insight for future studies of drug-receptor interactions including unwanted and unintended effects.

9. MATERIALS AND METHODS

Key Resources Table				
Reagent type (species) or resource	**Designation**	**Source or reference**	**Identifiers**	**Additional information**
Cell line (*Homo-sapiens*)	U2 OS (epithelial, osteosarcoma)	ATCC	HTB-96	
Antibody	Rabbit polyclonal anti-Flotillin1	Abcam	Ab41927	1:1000
Antibody	Rabbit monoclonal anti- Syntenin	Abcam	Ab133267	1:1000
Antibody	mouse monoclonal anti-CD63	Santa Cruz Biotechnology	sc-5275	1:1000
Antibody	mouse monoclonal anti-CD81	Santa Cruz Biotechnology	sc-166029	1:500
Antibody	Rabbit polyclonal anti-CD9	Abcam	ab223052	1:1000
Antibody	Rabbit polyclonal anti-calnexin	Abcam	ab22595	1:1000
Antibody	Rabbit monoclonal anti-phospho-ERK1/2 (pERK1/2)	MilliporeSigma	05-797R	1:1000
Antibody	Rabbit polyclonal anti-p44/42 MAPK (total ERK1/2)	Cell Signaling Technology	9102	1:1000

Antibody	Mouse monoclonal anti-β-actin	Santa Cruz Biotechnology	sc-69879	1:1000
sequence-based reagent	Megaplex RT primer human pool set V3.0	Thermo Fisher Scientific	4444750	
sequence-based reagent	Megaplex PreAmp primers human pool set V3.0	Thermo Fisher Scientific	4444748	
sequence-based reagent	TaqMan Array Human MicroRNA A+B Card Set v3.0	Thermo Fisher Scientific	4444913	
peptide, recombinant protein	Human recombinant SDF-1α	MilliporeSigma	GF344	
peptide, recombinant protein	Human recombinant Wnt3a	MilliporeSigma	H17001	
Commercial assay or kit	cAMP EIA kit	Cayman Chemical	581001	
Commercial assay or kit	ALP assay kit	Abcam	ab83369	
Commercial assay or kit	Cisbio IP-1 Elisa kit	Revvity	72IP1PEA	
Commercial assay or kit	MagMax mirVana total RNA isolation kit	Applied Biosystems, Thermo Fisher Scientific	A27828	
Commercial assay or kit	Qubit miRNA assay kit	Thermo Fisher Scientific	Q32880	

Chemical compound, drug	Di8-ANEPPS	Thermo Fisher Scientific	D3167	
Chemical compound, drug	Fluronic F-127	Thermo Fisher Scientific	P3000MP	
Chemical compound, drug	2-Chloro-N^6-cyclopentyladenosine (CCPA)	Tocris Bioscience	1705	
Chemical compound, drug	8-Cyclopentyl-1,3-dipropylxanthine (DPCPX)	Tocris Bioscience	0439	
Chemical compound, drug	2-pyridylethylamine dihydrochloride	Tocris Bioscience	2478	
Chemical compound, drug	Cetirizine dihydrochloride	Tocris Bioscience	2577	
software, algorithm	GraphPAD Prism software version 10	GraphPAD Software Inc.		
software, algorithm	SR plot web service	https://www.bioinformatics.com.cn/srplot		
software, algorithm	miRNet online web service v2.0	http://www.mirnet.ca		
software, algorithm	CytoScape software (V3.10.1)	https://cytoscape.org		

Drugs and reagents

CCPA, the selective adenosine A_1 receptor agonist, and adenosine A_1 receptor antagonist, DPCPX, were obtained from Tocris Bioscience (Minneapolis, MN). 2-pyridylethylamine dihydrochloride (PEA), the agonist of the histamine H_1 receptor, and cetirizine dihydrochloride, the antagonist of H_1 receptor were obtained from Tocris Bioscience (Minneapolis, MN). CCPA and DPCPX were diluted in DMSO, then subsequently diluted in the cell culture medium with a final DMSO concentration of 0.01%. Both 2-pyridylethylamine dihydrochloride and cetirizine dihydrochloride were diluted in water. Human recombinant Wnt3a protein and SDF-1α were obtained from Sigma (Burlington, MA). Wnt3a and SDF-1α were reconstituted to 100μg/ml in sterile 1XPBS containing 0.1% human serum albumin (HSA) at 100μg/ml. Wnt3a and SDF-1α were subsequently diluted in the cell culture medium with a final HSA concentration of 0.0001%. Gibco exosome-depleted fetal bovine serum (FBS) was purchased from ThermoFisher (A2720801, Thermo Fisher Scientific, Waltham, MA). Then the FBS were further charcoal-stripped to remove the potential GPCR agonists in the serum.

Cell culture

U2OS cells purchased from ATCC (Cat. No. HTB-96) were grown in McCoy 5A medium (16600082, Gibco, Thermo Fisher Scientific) supplemented with 10% fetal clone serum (FCS) and 1% penicillin and streptomycin and maintained in a humidified incubator with 10% CO_2 according to ATCC instructions. For EV isolation, cells were plated at $6x10^6$ in a 15 cm culture dish two days before the experiment. On the day of the experiment, cells were rinsed with 1XPBS, then treated with agonists or vehicle control in the medium containing 10% EV-depleted and charcoal-stripped FBS. The treatments were left on for 24 hours before medium collection for EV isolation. Four 15 cm plates with a total medium volume of 55 ml of each condition were used for EV isolation.

cAMP accumulation assay

U2OS cells were plated at $4x10^5$/well in the 24-well plate two days before the assay. One day before the assay, cells were switched to the culture medium containing 10% charcoal-stripped FCS and incubated overnight. The assay procedure and buffer are as previously described (Watts et al., 1998). CCPA (10^{-9} to 10^{-4}) was added to the cells and the plates were incubated for 20 min at 37°C in a humidified incubator with 5% CO_2. For the experiment with the antagonist, DPCPX (5 μM) was added to the cells and preincubated for 10 min before CCPA addition. cAMP accumulation was measured using cAMP EIA kit from Cayman Chemical (581001, Ann Arbor, MI), according to the manufacturer's instructions. All the experiments were conducted with three biological repeats, each performed with duplicated determinants.

Inositol monophosphate formation

U2OS cells were plated at $4x10^5$/well in the 24-well plate one day before the assay in the culture medium containing 10% charcoal-stripped FCS. The next day, cells were starved with plain McCoy 5A medium for 1 hour before the assay. Cells were preincubated with stimulation buffer for 10 min before agonist addition. Pyridylethylamine (10^{-8} to 10^{-3}) was added to the cells and the plates were incubated for 60min at 37°C in a humidified incubator with 5% CO_2. For the experiment with the antagonist, Cetirizine (1 μM) was preincubated for 10min before agonist addition. The accumulation of inositol monophosphate was measured using the Cisbio IP-1 Elisa kit (72IP1PEA, Revvity, Waltham, MA) as described previously (Eshleman et al., 2013). All the experiments were conducted with three independent repeats, each performed with duplicate determinants.

Alkaline phosphatase assay

U2OS cells were seeded at $4x10^5$/well in the 12 well-plate one day before the agonist treatment. Cells were treated with vehicle control (HSA) or various doses of Wnt3a diluted in cell culture medium and incubated for 24 hours. On the day of the assay, cells were rinsed with ice-cold 1XPBS and kept on the wet ice all the time. Cells were scraped and collected with 100 μl assay buffer/well, then transferred to microcentrifuge tubes. The cell suspensions were homogenized for 15-20 seconds with the micro pestle

homogenizer. The lysates were centrifuged 13,000xg for 20 min at 4°C to remove insoluble material. Alkaline phosphatase (ALP) activity was measured using the ALP assay kit (ab83369, Abcam, Waltham, MA). Briefly, 80 µl of cell lysate aliquot/well was mixed with kit reagent, then the plate was incubated at 25°C for 60 min. 10 µl of cell lysate was used to measure total protein concentration, which is used to normalize the enzyme activity. All the experiments were conducted with three independent repeats, each performed with duplicate determinants.

EV isolation by size exclusion chromatography

To determine which fractions are EV-enriched, 30ml of the medium control (plain medium with 10% EV-depleted FBS) and 30ml of the conditioned medium from two 15cm plates of U2OS cells incubated for 24 hours were collected and centrifuged at 300xg at 4°C for 15 min to remove cells and cell debris. The EV isolation methods were adapted from Benedikter et al 2017 (Benedikter et al., 2017). The supernatants were collected and centrifuged at 4000xg at 4°C for 15 min to further remove cell debris. After the second spin, the supernatants were passed through a 0.22µM Millipore Steriflip filter (Burlington, MA). Then media were loaded on a 2% Tween precoated Amicon Ultra-15 centrifugal filter unit with Ultracel-10 membrane (MWCO=10kDa, Millipore, Burlington, MA). The media were concentrated to ~550 µl by repeated centrifuge (4000xg) at 4°C. The concentrated media were fractionated by using size exclusion chromatography (SEC) (Izon qEV Original/35nM, IZON Science, Medford, MA) according to the manufacturer's instructions. Briefly, 500 µl of concentrated media were loaded to the qEV column. 12 fractions of 0.5 ml each eluted with 1XPBS (0.1uM filtered) were collected. Individual fractions were concentrated with Microcon-30 kDa Centrifugal Filters (Millipore, Burlington, MA) to a final volume of 70 µl and stored at -80°C for immunoblot.

For further miRNA assessment, 60ml of conditioned media pooled from four 15 cm plates per condition were harvested after 24 hours incubation of U2OS cells with agonists or vehicle control. For each GPCR, the experiments included 6 replicates of the agonist treatment group, 6 replicates of vehicle control (VC) and 6-8 replicates of media control (MC). The EV-enriched fractions 7, 8, and 9 (with a total volume of

1.5ml) were pooled for transmission electron microscopy (TEM), nanoparticle tracking analysis (NTA) and total RNA isolation. Pooled fractions were aliquoted and stored at -80°C until processed. Fractions used for TEM were stored at 4°C.

Immunoblotting

To evaluate the EV-enriched SEC fractions, 500µl of void (pooled fraction 1-6) and individual fractions 7 to 12 were concentrated with Microcon-30 kDa Centrifugal Filters (Millipore, Burlington, MA) to a final volume of 70 µl. Due to the undetectable protein amount in the concentrated fractions, an equal volume (30 µl) for each fraction was subjected to SDS-PAGE through 12% polyacrylamide gels and transferred to polyvinylidene fluoride (PVDF) membranes (BioRad, Hercules CA). Membranes were blocked with 5% non-fat dry milk in TBST at room temperature for 30 min, and then subsequently incubated at 4°C overnight with rabbit anti-flotillin (1:1000, ab41927, Abcam, Waltham, MA), rabbit anti-syntenin (1:1000, ab133267, Abcam, Waltham, MA), mouse anti-CD63 (1: 1000, sc-5275, Santa Cruz Biotechnology), mouse anti-CD81(1:500, sc-166029, Santa Cruz Biotechnology), rabbit anti-CD9 (1: 1000, ab223052, Abcam, Waltham, MA), rabbit anti-calnexin (1:1000, ab22595, Abcam, Waltham, MA). The immunoblots were rinsed and incubated with HRP-conjugated secondary antibodies. Immune complexes were visualized by chemiluminescence and analyzed using Bio-Rad ChemiDoc Imager. Bands were analyzed by densitometry using Bio-Rad Image lab software.

For the ACKR3 functional assay, cell lysates with a total of 15 µg protein of each condition were loaded into the gel. The immunoblots were incubated overnight with rabbit anti-pERK1/2 (1:1000, 05-797R, MilliporeSigma, Burlington MA), rabbit anti-tERK1/2 (1:1000, 9102, Cell Signaling Technology, Danvers MA), and mouse anti-β-actin (1:1000, sc-69879, Santa Cruz Biotechnology, Dallas Texas). β-actin was used as an internal control.

Transmission electron microscopy of EVs

15 µl of EV pooled fractions 7 to 9 were mixed with 5 µl of 16% paraformaldehyde and kept on the wet ice until processed. 5 µl of EV preparations were deposited and incubated for 3 minutes onto glow discharged copper grids (Ted Pella 01822-F). After this incubation period the grids were rinsed 15 seconds in distilled water, wicked on Whatman filter paper #1, and then stained for 3 minutes in freshly prepared 1% (w/v) aqueous uranyl acetate. Grids were then wicked with filter paper and air dried. Samples containing EVs were imaged at 120 kV on a FEI Tecnai™ Spirit TEM system. Images were acquired on an Advanced Microscopy Techniques (AMT) Nanosprint12 cMOS 12-megapixel camera system as tiff files.

Fluorescence nanoparticle tracking analysis (f-NTA)

SEC EVs (pooled void volume fraction1-6 and pooled EV enriched fraction 7-9) from controlled media and media from U2OS cells were analyzed for particle concentration and size by ZetaView nanoparticle tracking analyzer (Particle Metrix, Ammersee Germany) as described by the manufacture's protocol. Briefly, EV samples were labeled with fluorescent membrane dye Di8-ANEPPS (D3167, Thermo Fisher Scientific, Waltham, MA), staining solution (12 µM) supplemented with Fluronic F-127 (P3000MP Thermo Fisher Scientific, Waltham, MA) at room temperature for 15 min. The samples were diluted at 1:200 in 0.1 µM filtered 0.1X PBS in a final volume of 1ml for injection. Before the measurement, the instrument was calibrated with 100 nm polystyrene beads (Particle Metrix, Cat no 110-0020). The EV samples were recorded for 90s at controlled room temperature. All measurements were done in triplicates. ZetaView software was used to quantify the concentration (particles/ml) and size distribution (nm) of the particles.

EV RNA isolation and miRNA array

Pooled EV-enriched fractions (7,8 and 9, total of 1.3ml) were concentrated with Microcon-30 kDa Centrifugal Filters (Millipore, Burlington, MA) to a final volume of 250 µl and used for EV RNA isolation. The total RNAs were isolated using MagMax mirVana total RNA isolation kit (A27828, Applied Biosystems, ThermoFisher Scientific) according to manufacturer's instructions. The miRNA

concentration of each sample was measured with the Qubit miRNA assay kit (Q32880, ThermoFisher Scientific). The isolated RNA was stored at -80°C until processing. The reverse transcription and pre-amplification reactions were run as previously described (Sandau et al., 2020). Briefly, RNA (with 8-10 ng of miRNA) was reverse transcribed using Megaplex RT primer human pool set V3.0 (4444750, ThermoFisher Scientific) and MultiScribe Reverse Transcriptase (4311235, ThermoFisher Scientific) according to the user guide. To increase the sensitivity of qPCR analysis for miRNA targets, cDNA was pre-amplified (14 cycles) with Megaplex PreAmp primers human pool set V3.0 (4444748, ThermoFisher Scientific) and TaqMan PreAmp Master mix (4391128, ThermoFisher Scientific). Before the qPCR, pre-amplified cDNA was diluted 1:1 in nuclease-free water, then mixed with TaqMan Universal Master Mix (444047, ThermoFisher Scientific). The samples were loaded to TaqMan Array Human MicroRNA A+B Card Set v3.0 (4444913, ThermoFisher Scientific), which contains a total of 754 miRNA assays. The PCR amplification and data acquisition were carried out using the QuantStudio 12K Flex real-time PCR system (ThermoFisher Scientific).

miRNA array and analysis

MiRNA expression was analyzed using relative quantification methods as previously described (Sandau et al., 2020). The Cq value for each well along with the amplification score (AmpScore) and Cq confidence (CqConf) was reported by ExpressionSuit Software v1.3 (ThermoFisher). Amplifications were filtered prior to the data analysis, as follows: PCR products with Cq > 34, CqConf < 0.8, or AmpScore < 1 were excluded and treated as missing values. Only expressed miRNAs meeting these criteria in more than 80% of both vehicle control and treatment group samples were accepted for further analysis. To maximize accuracy and minimize amplification variation between the A and B cards, a mean expression value calculated from qualified miRNAs pooled from both the A and B cards was used to normalize the PCR data. miRNAs chosen for calculating mean expression for endogenous background normalization had to meet the following criteria: (1) the miRNA was not expressed or was observed in less than 50% of the untreated media, (2) was consistently fully observed in all vehicle control and treated samples and (3)

for miRNAs observed at rates of less than 50% in untreated media, the Cq value of the media control was required to be > 3.3 cycles different from the vehicle control. The mean expression Cq value of all the qualified miRNAs was calculated and used for endogenous background normalization. The ΔCq value for a miRNA was calculated as: ΔCq = Cq value of the miRNA – mean normalizer Cq value in the same group. The ΔΔCq value for a miRNA was calculated as: ΔΔCq = ΔCq for treated samples – ΔCq for vehicle control samples. The fold change (relative quantification value) for each miRNA was calculated as: $2^{-\Delta\Delta Cq}$. A relative quantification value > 1 indicates increased miRNA expression in the treated samples compared to vehicle control, and a relative quantification value < 1 indicates decreased miRNA expression in the treated samples.

Data analysis and statistical analysis

Dose-response curves for cAMP and IP1 accumulation were analyzed by nonlinear regression. Significant differences were determined by two-way analysis of variance (ANOVA) of receptors by agonist or antagonist concentration followed by Sidak's multiple comparison test. For the ALP accumulation and ERK1/2 activation, the significant differences were assessed by one-way ANOVA followed by Tukey's multiple comparison test. All functional assay data were shown as mean ± SD. The statistical significance in EV concentrations was determined using Student's *t*-test. Data were expressed as mean ± SEM. Data were analyzed with GraphPAD Prism software v10 (GraphPAD Software Inc., San Diego, CA). Statistical tests were applied based on three independent replicates. P values < 0.05 were considered significant.

To statistically evaluate the qPCR miRNA expression data, we elected to use strongly unbiased robust procedures including matched-pairs estimators of the effect sizes and rank-based testing of associations in the interest of minimizing confounding of associations by technical causes, and then to further interrogate those results with extensive sensitivity analyses designed to probe the volatility of the conclusions

depending on our choice of analytical methods. For example, as an alternative normalization procedure to relax the assumption (needed for validity of per-run normalization) of no differential measurement drift and to mitigate the run-to-run volatility of normalizer mean estimation we considered aligning median normalizer scores by treatment group rather than explicitly adjusting qPCR runs for each sample, but observed that residual technical variance (in the aligned normalizer scores) between matched pairs was actually increased due to the complications of missing data created by quality filtering, the technical run-batching of the assay into A and B cards, varying qPCR performance of even the endogenous normalizer miRNAs across runs, and other technical factors beyond our control.

To estimate the treatment effects on miRNA and calculate robust p-values for testing of those effects, we considered six different combinations of treatment effect estimator and p-value estimator in sensitivity analyses (Supplemental Fig. S1); Each of the approaches offers an alternative estimate of the magnitude and significance of the ΔΔCq value, varying depending on how pairs and treatment groups and batches are aggregated or disaggregated. We consider the matched-pairs estimator (Allison, 2009) of treatment effect superior to other approaches because of its strong unbiasedness even in the presence of technical confounding, and the Skillings-Mack estimator (Skillings & Mack, 1981) of the p-value superior both to naïve permutation-based (Good, 2006) or rank-based tests (Mann & Whitney, 1947) and to Welch's robust t-test (Welch, 1947) because it explicitly accounts for imbalanced group sizes (in our case caused by missing data at the per-miRNA level).

Ranking of miRNAs within each receptor type was first performed by magnitude of treatment effect (in normalized ΔCq units), as estimated from the matched-pairs regression approach, and the ranking was then filtered by the Skillings-Mack p-value. Because of the first-in-practice exploratory nature of this study we opted to emphasize discovery power over avoidance of false positives, and thus chose a liberal

cutoff of $p < 0.2$ for selection of associated miRNAs for further investigation. Pathway enrichment and functional annotation analyses were limited to the subset of miRNAs highlighted as the most-affected for each receptor; the cutoff for this was absolute fold change ≥ 1.5 ($|\Delta\Delta Cq| \geq 0.585$) for agonist versus vehicle control. The $\log_2$ fold change, Skillings-Mack p-values, and z-transformed $\log_2$ fold change values (Z-Score) were used to create volcano plots and hierarchical heatmaps. The hierarchical clustering in the heatmap is based on Euclidean distance. The visualizations were generated using GraphPad Prism v.10 and SR plot web service (https://www.bioinformatics.com.cn/srplot).

miRNA targets and pathway analysis

Prediction of miRNA targets was conducted using miRNet online web service v2.0 (http://www.mirnet.ca). The miRNA-target interactions were analyzed using the experimentally validated miRNA-target interaction databases: miRTarbase (v8.0) and Tarbase (v8.0). Human transcripts targeted by at least two miRNAs from each receptor were exported for further functional analysis. The target gene lists were submitted to String (v12.0) and GeneOntology with default settings to identify pathways enriched with miRNA targets and construct PPI networks. Kyoto Encyclopedia of Genes and Genomes (KEGG) pathway enrichment analyses and WikiPathway analyses were performed with String (v12.0) using the hypergeometric algorithm and the statistically enriched terms were determined by Fisher's exact test with adjusted *p*-value (false discovery rate) < 0.05 as the threshold. To measure the enrichment effect, the pathways were sorted by $\log_{10}$(observed/expected), which is the ratio between the number of proteins in our observed network that are annotated with a term and the number of the proteins that the software expects to be annotated with the same term in a random network of the similar size. Pathways exhibiting significant changes were further visualized with bubble plots using the SR plot web service (https://www.bioinformatics.com.cn/srplot). The PPI networks constructed by String were analyzed with CytoScape software (V3.10.1). The hub genes were identified and selected using CytoHubba, a plug-in of CytoScape, according to the node degree in the PPI network.

10. ACKNOWLEDGEMENTS: We thank Dr. Alfred Lewy, Dr. Kim Neve, and Dr. Atheir Abbas for critically reading the manuscript. We also acknowledge the OHSU Gene Profiling Shared Resource for providing the technical support for the qPCR assays. Transmission electron microscopy was performed at the Multiscale Microscopy Core, a member of the OHSU University Shared Resource Cores (RRID:SCR_022652) under the guidance of Dr. Claudia S. Lopez.

11. DATA AND MATERIALS AVAILABILITY: The microRNA array data is MIAME compliant and have been deposited to the Gene expression Omnibus site: http:// www.ncbi.nlm.nih.gov/geo/. GEO accession numbers: GSE270077, GSE270078, GSE270079, and GSE270080. All data needed to evaluate the conclusions in the paper are present in the paper or in the Supplemental Materials. Materials are available upon request from the corresponding author.

12. AUTHOR CONTRIBUTIONS: Conceptualization, X.S., M.C.P, and A.J.; investigation and methodology X.S., M.C.P, S.B., J.W., S.M., and A.J.; manuscript writing, editing, and reviewing X.S., M.C.P, S.B., J.W., S.M., and A.J.; funding acquisition A.J.

13. FOOTNOTE

Funding: This work was supported by funding from T32AG055378-06 (M.C.P), NIDA ADA 12013 (A.J.), FDA CDER-20-I—0546 (A.J.), DEA D-15-0D-002 (A.J.), Department of Veterans Affairs 1IK6BX005754 (A.J.).

Competing Interests: The authors declare that they have no competing interests.

14. REFERENCES

Allison, P. (2009). *Fixed Effects Regression Models* https://doi.org/10.4135/9781412993869

Alonso, R., Mazzeo, C., Rodriguez, M. C., Marsh, M., Fraile-Ramos, A., Calvo, V., Avila-Flores, A., Merida, I., & Izquierdo, M. (2011). Diacylglycerol kinase α regulates the formation and polarisation of mature multivesicular bodies involved in the secretion of Fas ligand-containing exosomes in T lymphocytes. *Cell Death & Differentiation*, *18*(7), 1161-1173. https://doi.org/10.1038/cdd.2010.184

Ambrose, A. R., Alsahli, M. A., Kurmani, S. A., & Goodall, A. H. (2018). Comparison of the release of microRNAs and extracellular vesicles from platelets in response to different agonists. *Platelets*, *29*(5), 446-454. https://doi.org/10.1080/09537104.2017.1332366

Appert-Collin, A., Hubert, P., Crémel, G., & Bennasroune, A. (2015). Role of ErbB Receptors in Cancer Cell Migration and Invasion. *Front Pharmacol*, *6*, 283. https://doi.org/10.3389/fphar.2015.00283

Arthofer, E., Hot, B., Petersen, J., Strakova, K., Jäger, S., Grundmann, M., Kostenis, E., Gutkind, J. S., & Schulte, G. (2016). WNT Stimulation Dissociates a Frizzled 4 Inactive-State Complex with Gα12/13. *Mol Pharmacol*, *90*(4), 447-459. https://doi.org/10.1124/mol.116.104919

Asher, W. B., Terry, D. S., Gregorio, G. G. A., Kahsai, A. W., Borgia, A., Xie, B., Modak, A., Zhu, Y., Jang, W., Govindaraju, A., Huang, L. Y., Inoue, A., Lambert, N. A., Gurevich, V. V., Shi, L., Lefkowitz, R. J., Blanchard, S. C., & Javitch, J. A. (2022). GPCR-mediated β-arrestin activation deconvoluted with single-molecule precision. *Cell*, *185*(10), 1661-1675.e1616. https://doi.org/10.1016/j.cell.2022.03.042

Bebelman, M. P., Crudden, C., Pegtel, D. M., & Smit, M. J. (2020). The Convergence of Extracellular Vesicle and GPCR Biology. *Trends Pharmacol Sci*, *41*(9), 627-640. https://doi.org/10.1016/j.tips.2020.07.001

Benedikter, B. J., Bouwman, F. G., Vajen, T., Heinzmann, A. C. A., Grauls, G., Mariman, E. C., Wouters, E. F. M., Savelkoul, P. H., Lopez-Iglesias, C., Koenen, R. R., Rohde, G. G. U., & Stassen, F. R. M. (2017). Ultrafiltration combined with size exclusion chromatography efficiently isolates extracellular vesicles from cell culture media for compositional and functional studies. *Sci Rep*, *7*(1), 15297. https://doi.org/10.1038/s41598-017-15717-7

Bhattacharya, P., Dhawan, U. K., Hussain, M. T., Singh, P., Bhagat, K. K., Singhal, A., Austin-Williams, S., Sengupta, S., & Subramanian, M. (2023). Efferocytes release extracellular vesicles to resolve inflammation and tissue injury via prosaposin-GPR37 signaling. *Cell Rep*, *42*(7), 112808. https://doi.org/10.1016/j.celrep.2023.112808

Bost, J. P., Saher, O., Hagey, D., Mamand, D. R., Liang, X., Zheng, W., Corso, G., Gustafsson, O., Görgens, A., Smith, C. E., Zain, R., El Andaloussi, S., & Gupta, D. (2022). Growth Media Conditions Influence the Secretion Route and Release Levels of Engineered Extracellular Vesicles. *Adv Healthc Mater*, *11*(5), e2101658. https://doi.org/10.1002/adhm.202101658

Bourgeois, B. L., Levitt, D. E., Molina, P. E., & Simon, L. (2023). Differential expression of adipocyte and myotube extracellular vesicle miRNA cargo in chronic binge alcohol-administered SIV-infected male macaques. *Alcohol*, *108*, 1-9. https://doi.org/10.1016/j.alcohol.2022.11.001

Brown, B. D., Gentner, B., Cantore, A., Colleoni, S., Amendola, M., Zingale, A., Baccarini, A., Lazzari, G., Galli, C., & Naldini, L. (2007). Endogenous microRNA can be broadly exploited to regulate

transgene expression according to tissue, lineage and differentiation state. *Nature Biotechnology*, *25*(12), 1457-1467. https://doi.org/10.1038/nbt1372

Chao, Y., Gu, T., Zhang, Z., Wu, T., Wang, J., & Bi, Y. (2023). The role of miRNAs carried by extracellular vesicles in type 2 diabetes and its complications. *J Diabetes*. https://doi.org/10.1111/1753-0407.13456

Chen, H., Qiao, H., Zhao, Q., & Wei, F. (2022). microRNA-135a-5p regulates NOD-like receptor family pyrin domain containing 3 inflammasome-mediated hypertensive cardiac inflammation and fibrosis via thioredoxin-interacting protein. *Bioengineered*, *13*(3), 4658-4673. https://doi.org/10.1080/21655979.2021.2024956

Cheung, L., Zervou, S., Mattsson, G., Abouna, S., Zhou, L., Ifandi, V., Pelengaris, S., & Khan, M. (2010). c-Myc directly induces both impaired insulin secretion and loss of β-cell mass, independently of hyperglycemia in vivo. *Islets*, *2*(1), 37-45. https://doi.org/10.4161/isl.2.1.10196

Conrad, K. P., Tuna, K. M., Mestre, C. T., Banwatt, E. S., & Alli, A. A. (2020). Activation of multiple receptors stimulates extracellular vesicle release from trophoblast cells. *Physiol Rep*, *8*(20), e14592. https://doi.org/10.14814/phy2.14592

Crawford, M., Ford, S., Henry, M., Matherne, G. P., & Lankford, A. (2005). Myocardial function following cold ischemic storage is improved by cardiac-specific overexpression of A1-adenosine receptors. *Can J Physiol Pharmacol*, *83*(6), 493-498. https://doi.org/10.1139/y05-038

Doyle, L. M., & Wang, M. Z. (2019). Overview of Extracellular Vesicles, Their Origin, Composition, Purpose, and Methods for Exosome Isolation and Analysis. *Cells*, *8*(7). https://doi.org/10.3390/cells8070727

Eshleman, A. J., Wolfrum, K. M., Hatfield, M. G., Johnson, R. A., Murphy, K. V., & Janowsky, A. (2013). Substituted methcathinones differ in transporter and receptor interactions. *Biochem Pharmacol*, *85*(12), 1803-1815. https://doi.org/10.1016/j.bcp.2013.04.004

Evan, G. I., & Vousden, K. H. (2001). Proliferation, cell cycle and apoptosis in cancer. *Nature*, *411*(6835), 342-348. https://doi.org/10.1038/35077213

Fernández-Nogueira, P., Noguera-Castells, A., Fuster, G., Recalde-Percaz, L., Moragas, N., López-Plana, A., Enreig, E., Jauregui, P., Carbó, N., Almendro, V., Gascón, P., Bragado, P., & Mancino, M. (2018). Histamine receptor 1 inhibition enhances antitumor therapeutic responses through extracellular signal-regulated kinase (ERK) activation in breast cancer. *Cancer Letters*, *424*, 70-83. https://doi.org/https://doi.org/10.1016/j.canlet.2018.03.014

Fumagalli, A., Heuninck, J., Pizzoccaro, A., Moutin, E., Koenen, J., Séveno, M., Durroux, T., Junier, M. P., Schlecht-Louf, G., Bachelerie, F., Schütz, D., Stumm, R., Smit, M. J., Guérineau, N. C., Chaumont-Dubel, S., & Marin, P. (2020). The atypical chemokine receptor 3 interacts with Connexin 43 inhibiting astrocytic gap junctional intercellular communication. *Nat Commun*, *11*(1), 4855. https://doi.org/10.1038/s41467-020-18634-y

Gabay, M., Li, Y., & Felsher, D. W. (2014). MYC activation is a hallmark of cancer initiation and maintenance. *Cold Spring Harb Perspect Med*, *4*(6). https://doi.org/10.1101/cshperspect.a014241

Gelibter, S., Marostica, G., Mandelli, A., Siciliani, S., Podini, P., Finardi, A., & Furlan, R. (2022). The impact of storage on extracellular vesicles: A systematic study. *J Extracell Vesicles*, *11*(2), e12162. https://doi.org/10.1002/jev2.12162

Ginés, S., Ciruela, F., Burgueño, J., Casadó, V., Canela, E. I., Mallol, J., Lluís, C., & Franco, R. (2001). Involvement of caveolin in ligand-induced recruitment and internalization of A(1) adenosine receptor and adenosine deaminase in an epithelial cell line. *Mol Pharmacol*, *59*(5), 1314-1323.

Good, P. I. (2006). *Resampling methods: A practical guide to data analysis.* Birkhauser.

Görgens, A., Corso, G., Hagey, D. W., Jawad Wiklander, R., Gustafsson, M. O., Felldin, U., Lee, Y., Bostancioglu, R. B., Sork, H., Liang, X., Zheng, W., Mohammad, D. K., van de Wakker, S. I., Vader,

P., Zickler, A. M., Mamand, D. R., Ma, L., Holme, M. N., Stevens, M. M., . . . El Andaloussi, S. (2022). Identification of storage conditions stabilizing extracellular vesicles preparations. *J Extracell Vesicles*, *11*(6), e12238. https://doi.org/10.1002/jev2.12238

Hatipoglu, O. F., Nishinaka, T., Nishibori, M., Watanabe, M., Toyomura, T., Mori, S., Yaykasli, K. O., Wake, H., & Takahashi, H. (2023). Histamine promotes angiogenesis through a histamine H1 receptor-PKC-VEGF-mediated pathway in human endothelial cells. *Journal of Pharmacological Sciences*, *151*(4), 177-186. https://doi.org/https://doi.org/10.1016/j.jphs.2023.02.006

Heydenreich, F. M., Marti-Solano, M., Sandhu, M., Kobilka, B. K., Bouvier, M., & Babu, M. M. (2023). Molecular determinants of ligand efficacy and potency in GPCR signaling. *Science*, *382*(6677), eadh1859. https://doi.org/10.1126/science.adh1859

Horman, S. R., Janas, M. M., Litterst, C., Wang, B., MacRae, I. J., Sever, M. J., Morrissey, D. V., Graves, P., Luo, B., Umesalma, S., Qi, H. H., Miraglia, L. J., Novina, C. D., & Orth, A. P. (2013). Akt-mediated phosphorylation of argonaute 2 downregulates cleavage and upregulates translational repression of MicroRNA targets. *Mol Cell*, *50*(3), 356-367. https://doi.org/10.1016/j.molcel.2013.03.015

Im, E.-J., Lee, C.-H., Moon, P.-G., Rangaswamy, G. G., Lee, B., Lee, J. M., Lee, J.-C., Jee, J.-G., Bae, J.-S., Kwon, T.-K., Kang, K.-W., Jeong, M.-S., Lee, J.-E., Jung, H.-S., Ro, H.-J., Jun, S., Kang, W., Seo, S.-Y., Cho, Y.-E., . . . Baek, M.-C. (2019). Sulfisoxazole inhibits the secretion of small extracellular vesicles by targeting the endothelin receptor A. *Nature Communications*, *10*(1), 1387. https://doi.org/10.1038/s41467-019-09387-4

Jackson, L., Rennie, M., Poussaint, A., & Scarlata, S. (2022). Activation of Gαq sequesters specific transcripts into Ago2 particles. *Scientific Reports*, *12*(1), 8758. https://doi.org/10.1038/s41598-022-12737-w

Jin, Y., Ma, L., Zhang, W., Yang, W., Feng, Q., & Wang, H. (2022). Extracellular signals regulate the biogenesis of extracellular vesicles. *Biol Res*, *55*(1), 35. https://doi.org/10.1186/s40659-022-00405-2

Kahn, R., Mossberg, M., Ståhl, A. L., Johansson, K., Lopatko Lindman, I., Heijl, C., Segelmark, M., Mörgelin, M., Leeb-Lundberg, L. M., & Karpman, D. (2017). Microvesicle transfer of kinin B1-receptors is a novel inflammatory mechanism in vasculitis. *Kidney Int*, *91*(1), 96-105. https://doi.org/10.1016/j.kint.2016.09.023

Karlsson, M., Zhang, C., Méar, L., Zhong, W., Digre, A., Katona, B., Sjöstedt, E., Butler, L., Odeberg, J., Dusart, P., Edfors, F., Oksvold, P., von Feilitzen, K., Zwahlen, M., Arif, M., Altay, O., Li, X., Ozcan, M., Mardinoglu, A., . . . Lindskog, C. (2021). A single-cell type transcriptomics map of human tissues. *Sci Adv*, *7*(31). https://doi.org/10.1126/sciadv.abh2169

Kim, M. E., Kim, D. H., & Lee, J. S. (2022). FoxO Transcription Factors: Applicability as a Novel Immune Cell Regulators and Therapeutic Targets in Oxidative Stress-Related Diseases. *Int J Mol Sci*, *23*(19). https://doi.org/10.3390/ijms231911877

Kozielewicz, P., Shekhani, R., Moser, S., Bowin, C.-F., Wesslowski, J., Davidson, G., & Schulte, G. (2021). Quantitative Profiling of WNT-3A Binding to All Human Frizzled Paralogues in HEK293 Cells by NanoBiT/BRET Assessments. *ACS Pharmacology & Translational Science*, *4*(3), 1235-1245. https://doi.org/10.1021/acsptsci.1c00084

Kriebel, P. W., Majumdar, R., Jenkins, L. M., Senoo, H., Wang, W., Ammu, S., Chen, S., Narayan, K., Iijima, M., & Parent, C. A. (2018). Extracellular vesicles direct migration by synthesizing and releasing chemotactic signals. *J Cell Biol*, *217*(8), 2891-2910. https://doi.org/10.1083/jcb.201710170

Kritsilis, M., S, V. R., Koutsoudaki, P. N., Evangelou, K., Gorgoulis, V. G., & Papadopoulos, D. (2018). Ageing, Cellular Senescence and Neurodegenerative Disease. *Int J Mol Sci*, *19*(10). https://doi.org/10.3390/ijms19102937

Kugeratski, F. G., Hodge, K., Lilla, S., McAndrews, K. M., Zhou, X., Hwang, R. F., Zanivan, S., & Kalluri, R. (2021). Quantitative proteomics identifies the core proteome of exosomes with syntenin-1 as the highest abundant protein and a putative universal biomarker. *Nat Cell Biol*, *23*(6), 631-641. https://doi.org/10.1038/s41556-021-00693-y

Lam, E. W. F., Brosens, J. J., Gomes, A. R., & Koo, C.-Y. (2013). Forkhead box proteins: tuning forks for transcriptional harmony. *Nature Reviews Cancer*, *13*(7), 482-495. https://doi.org/10.1038/nrc3539

Lee, H., Li, C., Zhang, Y., Zhang, D., Otterbein, L. E., & Jin, Y. (2019). Caveolin-1 selectively regulates microRNA sorting into microvesicles after noxious stimuli. *J Exp Med*, *216*(9), 2202-2220. https://doi.org/10.1084/jem.20182313

Lee, Y. J., Shin, K. J., Jang, H. J., Ryu, J. S., Lee, C. Y., Yoon, J. H., Seo, J. K., Park, S., Lee, S., Je, A. R., Huh, Y. H., Kong, S. Y., Kwon, T., Suh, P. G., & Chae, Y. C. (2023). GPR143 controls ESCRT-dependent exosome biogenesis and promotes cancer metastasis. *Dev Cell*, *58*(4), 320-334.e328. https://doi.org/10.1016/j.devcel.2023.01.006

Lehrich, B. M., Liang, Y., & Fiandaca, M. S. (2021). Foetal bovine serum influence on in vitro extracellular vesicle analyses. *J Extracell Vesicles*, *10*(3), e12061. https://doi.org/10.1002/jev2.12061

Li, H., Xiao, Y., Li, Q., Yao, J., Yuan, X., Zhang, Y., Yin, X., Saito, Y., Fan, H., Li, P., Kuo, W. L., Halpin, A., Gibbons, D. L., Yagita, H., Zhao, Z., Pang, D., Ren, G., Yee, C., Lee, J. J., & Yu, D. (2022). The allergy mediator histamine confers resistance to immunotherapy in cancer patients via activation of the macrophage histamine receptor H1. *Cancer Cell*, *40*(1), 36-52.e39. https://doi.org/10.1016/j.ccell.2021.11.002

Li, Y. Z., Di Cristofano, A., & Woo, M. (2020). Metabolic Role of PTEN in Insulin Signaling and Resistance. *Cold Spring Harb Perspect Med*, *10*(8). https://doi.org/10.1101/cshperspect.a036137

Liu, Y., Hu, N., Ai, B., Xia, H., & Li, W. (2024). MiR-31-5p alleviates septic cardiomyopathy by targeting BAP1 to inhibit SLC7A11 deubiquitination and ferroptosis. *BMC Cardiovascular Disorders*, *24*(1), 286. https://doi.org/10.1186/s12872-024-03954-4

Liu, Y., Xu, Z., Zheng, H., Yang, J., Wu, M., Yang, Q., Wang, Y., Zong, T., Yang, X., Xie, T., Cai, J., Yao, Y., & Wang, X. (2023). MiR-423-5p promotes Müller cell activation via targeting NGF signaling in diabetic retinopathy. *Life Sci*, *334*, 122217. https://doi.org/10.1016/j.lfs.2023.122217

Mack, M., Kleinschmidt, A., Brühl, H., Klier, C., Nelson, P. J., Cihak, J., Plachý, J., Stangassinger, M., Erfle, V., & Schlöndorff, D. (2000). Transfer of the chemokine receptor CCR5 between cells by membrane-derived microparticles: a mechanism for cellular human immunodeficiency virus 1 infection. *Nat Med*, *6*(7), 769-775. https://doi.org/10.1038/77498

Majumder, M., Landman, E., Liu, L., Hess, D., & Lala, P. K. (2015). COX-2 Elevates Oncogenic miR-526b in Breast Cancer by EP4 Activation. *Mol Cancer Res*, *13*(6), 1022-1033. https://doi.org/10.1158/1541-7786.Mcr-14-0543

Mann, H. B., & Whitney, D. R. (1947). On a test of whether one of two random variables is stochastically larger than the other. *The annals of mathematical statistics*, 50-60.

Martins-Marques, T., Costa, M. C., Catarino, S., Simoes, I., Aasen, T., Enguita, F. J., & Girao, H. (2022). Cx43-mediated sorting of miRNAs into extracellular vesicles. *EMBO reports*, *23*(7). https://doi.org/10.15252/embr.202154312

Matthews, H. K., Bertoli, C., & de Bruin, R. A. M. (2022). Cell cycle control in cancer. *Nature Reviews Molecular Cell Biology*, *23*(1), 74-88. https://doi.org/10.1038/s41580-021-00404-3

Mazzeo, C., Calvo, V., Alonso, R., Mérida, I., & Izquierdo, M. (2016). Protein kinase D1/2 is involved in the maturation of multivesicular bodies and secretion of exosomes in T and B lymphocytes. *Cell Death & Differentiation*, *23*(1), 99-109. https://doi.org/10.1038/cdd.2015.72

McKenzie, A. J., Hoshino, D., Hong, N. H., Cha, D. J., Franklin, J. L., Coffey, R. J., Patton, J. G., & Weaver, A. M. (2016). KRAS-MEK Signaling Controls Ago2 Sorting into Exosomes. *Cell Rep*, *15*(5), 978-987. https://doi.org/10.1016/j.celrep.2016.03.085

Montastier, E., Beuzelin, D., Martins, F., Mir, L., Marqués, M. A., Thalamas, C., Iacovoni, J., Langin, D., & Viguerie, N. (2019). Niacin induces miR-502-3p expression which impairs insulin sensitivity in human adipocytes. *Int J Obes (Lond)*, *43*(7), 1485-1490. https://doi.org/10.1038/s41366-018-0260-5

Németh, A., Orgovan, N., Sódar, B. W., Osteikoetxea, X., Pálóczi, K., Szabó-Taylor, K. É., Vukman, K. V., Kittel, Á., Turiák, L., Wiener, Z., Tóth, S., Drahos, L., Vékey, K., Horvath, R., & Buzás, E. I. (2017). Antibiotic-induced release of small extracellular vesicles (exosomes) with surface-associated DNA. *Sci Rep*, *7*(1), 8202. https://doi.org/10.1038/s41598-017-08392-1

Nordin, J. Z. (2022). Transfection reagents affect Extracellular Vesicle cargo transfer to recipient cells: The importance of appropriate controls in EV research. *J Extracell Vesicles*, *11*(10), e12227. https://doi.org/10.1002/jev2.12227

Odegaard, K. E., Chand, S., Wheeler, S., Tiwari, S., Flores, A., Hernandez, J., Savine, M., Gowen, A., Pendyala, G., & Yelamanchili, S. V. (2020). Role of Extracellular Vesicles in Substance Abuse and HIV-Related Neurological Pathologies. *Int J Mol Sci*, *21*(18). https://doi.org/10.3390/ijms21186765

Ofer, D., & Linial, M. (2022). Inferring microRNA regulation: A proteome perspective. *Front Mol Biosci*, *9*, 916639. https://doi.org/10.3389/fmolb.2022.916639

Oliner, J. D., Saiki, A. Y., & Caenepeel, S. (2016). The Role of MDM2 Amplification and Overexpression in Tumorigenesis. *Cold Spring Harb Perspect Med*, *6*(6). https://doi.org/10.1101/cshperspect.a026336

Orr-Burks, N., Murray, J., Todd, K. V., Bakre, A., & Tripp, R. A. (2021). MicroRNAs affect GPCR and Ion channel genes needed for influenza replication. *J Gen Virol*, *102*(11). https://doi.org/10.1099/jgv.0.001691

Ortega, F. J., Mercader, J. M., Catalán, V., Moreno-Navarrete, J. M., Pueyo, N., Sabater, M., Gómez-Ambrosi, J., Anglada, R., Fernández-Formoso, J. A., Ricart, W., Frühbeck, G., & Fernández-Real, J. M. (2013). Targeting the circulating microRNA signature of obesity. *Clin Chem*, *59*(5), 781-792. https://doi.org/10.1373/clinchem.2012.195776

Palmisano, G., Jensen, S. S., Le Bihan, M. C., Lainé, J., McGuire, J. N., Pociot, F., & Larsen, M. R. (2012). Characterization of membrane-shed microvesicles from cytokine-stimulated β-cells using proteomics strategies. *Mol Cell Proteomics*, *11*(8), 230-243. https://doi.org/10.1074/mcp.M111.012732

Palumbo, M. C., Gautam, M., Sonneborn, A., Kim, K., Wilmarth, P. A., Reddy, A. P., Shi, X., Marks, D. L., Sahay, G., Abbas, A. I., & Janowsky, A. (2023). MicroRNA137-loaded lipid nanoparticles regulate synaptic proteins in the prefrontal cortex. *Molecular Therapy*, *31*(10), 2975-2990. https://doi.org/https://doi.org/10.1016/j.ymthe.2023.08.016

Palviainen, M., Saari, H., Kärkkäinen, O., Pekkinen, J., Auriola, S., Yliperttula, M., Puhka, M., Hanhineva, K., & Siljander, P. R. (2019). Metabolic signature of extracellular vesicles depends on the cell culture conditions. *J Extracell Vesicles*, *8*(1), 1596669. https://doi.org/10.1080/20013078.2019.1596669

Panjehpour, M., Castro, M., & Klotz, K. N. (2005). Human breast cancer cell line MDA-MB-231 expresses endogenous A2B adenosine receptors mediating a Ca2+ signal. *Br J Pharmacol*, *145*(2), 211-218. https://doi.org/10.1038/sj.bjp.0706180

Papadopoulos, D., Magliozzi, R., Mitsikostas, D. D., Gorgoulis, V. G., & Nicholas, R. S. (2020). Aging, Cellular Senescence, and Progressive Multiple Sclerosis. *Front Cell Neurosci*, *14*, 178. https://doi.org/10.3389/fncel.2020.00178

Park, C., Lee, J.-W., Kim, K., Seen, D.-S., Jeong, J.-Y., & Huh, W.-K. (2023). Simultaneous activation of CXC chemokine receptor 4 and histamine receptor H1 enhances calcium signaling and cancer cell migration. *Scientific Reports*, *13*(1), 1894. https://doi.org/10.1038/s41598-023-28531-1

Park, C., Lee, J. W., Kim, K., Seen, D. S., Jeong, J. Y., & Huh, W. K. (2023). Simultaneous activation of CXC chemokine receptor 4 and histamine receptor H1 enhances calcium signaling and cancer cell migration. *Sci Rep*, *13*(1), 1894. https://doi.org/10.1038/s41598-023-28531-1

Patel, S., Doble, B. W., MacAulay, K., Sinclair, E. M., Drucker, D. J., & Woodgett, J. R. (2008). Tissue-specific role of glycogen synthase kinase 3beta in glucose homeostasis and insulin action. *Mol Cell Biol*, *28*(20), 6314-6328. https://doi.org/10.1128/mcb.00763-08

Perez-Vilar, J., & Hill, R. L. (1997). Norrie Disease Protein (Norrin) Forms Disulfide-linked Oligomers Associated with the Extracellular Matrix*. *Journal of Biological Chemistry*, *272*(52), 33410-33415. https://doi.org/https://doi.org/10.1074/jbc.272.52.33410

Pfeffer, C. M., & Singh, A. T. K. (2018). Apoptosis: A Target for Anticancer Therapy. *Int J Mol Sci*, *19*(2). https://doi.org/10.3390/ijms19020448

Pham, C. V., Midge, S., Barua, H., Zhang, Y., Ngoc-Gia Nguyen, T., Barrero, R. A., Duan, A., Yin, W., Jiang, G., Hou, Y., Zhou, S., Wang, Y., Xie, X., Tran, P. H. L., Xiang, D., & Duan, W. (2021). Bovine extracellular vesicles contaminate human extracellular vesicles produced in cell culture conditioned medium when 'exosome-depleted serum' is utilised. *Archives of Biochemistry and Biophysics*, *708*, 108963. https://doi.org/https://doi.org/10.1016/j.abb.2021.108963

Plotnikova, O., Baranova, A., & Skoblov, M. (2019). Comprehensive Analysis of Human microRNA-mRNA Interactome. *Front Genet*, *10*, 933. https://doi.org/10.3389/fgene.2019.00933

Reichelt, M. E., Willems, L., Molina, J. G., Sun, C. X., Noble, J. C., Ashton, K. J., Schnermann, J., Blackburn, M. R., & Headrick, J. P. (2005). Genetic deletion of the A1 adenosine receptor limits myocardial ischemic tolerance. *Circ Res*, *96*(3), 363-367. https://doi.org/10.1161/01.Res.0000156075.00127.C3

Ripke, S., Neale, B. M., Corvin, A., Walters, J. T. R., Farh, K.-H., Holmans, P. A., Lee, P., Bulik-Sullivan, B., Collier, D. A., Huang, H., Pers, T. H., Agartz, I., Agerbo, E., Albus, M., Alexander, M., Amin, F., Bacanu, S. A., Begemann, M., Belliveau Jr, R. A., . . . Psychosis Endophenotypes International, C. (2014). Biological insights from 108 schizophrenia-associated genetic loci. *Nature*, *511*(7510), 421-427. https://doi.org/10.1038/nature13595

Rothman, J. E. (1996). The protein machinery of vesicle budding and fusion. *Protein Sci*, *5*(2), 185-194. https://doi.org/10.1002/pro.5560050201

Ryzhov, S., Matafonov, A., Galindo, C. L., Zhang, Q., Tran, T. L., Lenihan, D. J., Lenneman, C. G., Feoktistov, I., & Sawyer, D. B. (2017). ERBB signaling attenuates proinflammatory activation of nonclassical monocytes. *Am J Physiol Heart Circ Physiol*, *312*(5), H907-h918. https://doi.org/10.1152/ajpheart.00486.2016

Sandau, U. S., Duggan, E., Shi, X., Smith, S. J., Huckans, M., Schutzer, W. E., Loftis, J. M., Janowsky, A., Nolan, J. P., & Saugstad, J. A. (2020). Methamphetamine use alters human plasma extracellular vesicles and their microRNA cargo: An exploratory study. *J Extracell Vesicles*, *10*(1), e12028. https://doi.org/10.1002/jev2.12028

Sandau, U. S., McFarland, T. J., Smith, S. J., Galasko, D. R., Quinn, J. F., & Saugstad, J. A. (2022). Differential Effects of APOE Genotype on MicroRNA Cargo of Cerebrospinal Fluid Extracellular Vesicles in Females With Alzheimer's Disease Compared to Males. *Front Cell Dev Biol*, *10*, 864022. https://doi.org/10.3389/fcell.2022.864022

Sarmoko, Toriyama, M., Kaji, N., & Itoh, H. (2025). Functional Analysis of Adhesion GPCR Latrophilin 2 (ADGRL2) in MDA-MB-231 Human Breast Cancer Cells. *Genes Cells*, *30*(4), e70030. https://doi.org/10.1111/gtc.70030

Shi, Z., Fultz, R. S., Engevik, M. A., Gao, C., Hall, A., Major, A., Mori-Akiyama, Y., & Versalovic, J. (2019). Distinct roles of histamine H1- and H2-receptor signaling pathways in inflammation-associated colonic tumorigenesis. *Am J Physiol Gastrointest Liver Physiol*, *316*(1), G205-g216. https://doi.org/10.1152/ajpgi.00212.2018

Sidhom, K., Obi, P. O., & Saleem, A. (2020). A Review of Exosomal Isolation Methods: Is Size Exclusion Chromatography the Best Option? *Int J Mol Sci*, *21*(18). https://doi.org/10.3390/ijms21186466

Sigismund, S., Avanzato, D., & Lanzetti, L. (2018). Emerging functions of the EGFR in cancer. *Mol Oncol*, *12*(1), 3-20. https://doi.org/10.1002/1878-0261.12155

Skillings, J. H., & Mack, G. A. (1981). On the use of a Friedman-type statistic in balanced and unbalanced block designs. *Technometrics*, *23*(2), 171-177.

Sriram, K., & Insel, P. A. (2018). G Protein-Coupled Receptors as Targets for Approved Drugs: How Many Targets and How Many Drugs? *Mol Pharmacol*, *93*(4), 251-258. https://doi.org/10.1124/mol.117.111062

Stevens, R. C., Cherezov, V., Katritch, V., Abagyan, R., Kuhn, P., Rosen, H., & Wüthrich, K. (2013). The GPCR Network: a large-scale collaboration to determine human GPCR structure and function. *Nat Rev Drug Discov*, *12*(1), 25-34. https://doi.org/10.1038/nrd3859

Strakova, K., Matricon, P., Yokota, C., Arthofer, E., Bernatik, O., Rodriguez, D., Arenas, E., Carlsson, J., Bryja, V., & Schulte, G. (2017). The tyrosine Y250(2.39) in Frizzled 4 defines a conserved motif important for structural integrity of the receptor and recruitment of Disheveled. *Cell Signal*, *38*, 85-96. https://doi.org/10.1016/j.cellsig.2017.06.018

Suelves, N., Saleki, S., Ibrahim, T., Palomares, D., Moonen, S., Koper, M. J., Vrancx, C., Vadukul, D. M., Papadopoulos, N., Viceconte, N., Claude, E., Vandenberghe, R., von Arnim, C. A. F., Constantinescu, S. N., Thal, D. R., Decottignies, A., & Kienlen-Campard, P. (2023). Senescence-related impairment of autophagy induces toxic intraneuronal amyloid-β accumulation in a mouse model of amyloid pathology. *Acta Neuropathol Commun*, *11*(1), 82. https://doi.org/10.1186/s40478-023-01578-x

Tabara, H., Yigit, E., Siomi, H., & Mello, C. C. (2002). The dsRNA binding protein RDE-4 interacts with RDE-1, DCR-1, and a DExH-box helicase to direct RNAi in C. elegans. *Cell*, *109*(7), 861-871. https://doi.org/10.1016/s0092-8674(02)00793-6

Tao, S., He, H., & Chen, Q. (2015). Estradiol induces HOTAIR levels via GPER-mediated miR-148a inhibition in breast cancer. *J Transl Med*, *13*, 131. https://doi.org/10.1186/s12967-015-0489-x

Tetta, C., Ghigo, E., Silengo, L., Deregibus, M. C., & Camussi, G. (2013). Extracellular vesicles as an emerging mechanism of cell-to-cell communication. *Endocrine*, *44*(1), 11-19. https://doi.org/10.1007/s12020-012-9839-0

Verweij, F. J., Bebelman, M. P., Jimenez, C. R., Garcia-Vallejo, J. J., Janssen, H., Neefjes, J., Knol, J. C., de Goeij-de Haas, R., Piersma, S. R., Baglio, S. R., Verhage, M., Middeldorp, J. M., Zomer, A., van Rheenen, J., Coppolino, M. G., Hurbain, I., Raposo, G., Smit, M. J., Toonen, R. F. G., . . . Pegtel, D. M. (2018). Quantifying exosome secretion from single cells reveals a modulatory role for GPCR signaling. *J Cell Biol*, *217*(3), 1129-1142. https://doi.org/10.1083/jcb.201703206

Verweij, F. J., Bebelman, M. P., Jimenez, C. R., Garcia-Vallejo, J. J., Janssen, H., Neefjes, J., Knol, J. C., De Goeij-De Haas, R., Piersma, S. R., Baglio, S. R., Verhage, M., Middeldorp, J. M., Zomer, A., Van Rheenen, J., Coppolino, M. G., Hurbain, I., Raposo, G., Smit, M. J., Toonen, R. F. G., . . . Pegtel, D. M. (2018). Quantifying exosome secretion from single cells reveals a modulatory role for GPCR signaling. *Journal of Cell Biology*, *217*(3), 1129-1142. https://doi.org/10.1083/jcb.201703206

Villarroya-Beltri, C., Gutiérrez-Vázquez, C., Sánchez-Cabo, F., Pérez-Hernández, D., Vázquez, J., Martin-Cofreces, N., Martinez-Herrera, D. J., Pascual-Montano, A., Mittelbrunn, M., & Sánchez-Madrid, F. (2013). Sumoylated hnRNPA2B1 controls the sorting of miRNAs into exosomes through binding to specific motifs. *Nat Commun*, *4*, 2980. https://doi.org/10.1038/ncomms3980

Wang, H. L., Wei, B., He, H. J., Huang, X. R., Sheng, J. Y., Chen, X. C., Wang, L., Tan, R. Z., Li, J. C., Liu, J., Yang, S. J., Ma, R. C., & Lan, H. Y. (2022). Smad3 deficiency improves islet-based therapy for diabetes and diabetic kidney injury by promoting β cell proliferation via the E2F3-dependent mechanism. *Theranostics*, *12*(1), 379-395. https://doi.org/10.7150/thno.67034

Wang, K. Y., Tanimoto, A., Yamada, S., Guo, X., Ding, Y., Watanabe, T., Watanabe, T., Kohno, K., Hirano, K., Tsukada, H., & Sasaguri, Y. (2010). Histamine regulation in glucose and lipid metabolism via histamine receptors: model for nonalcoholic steatohepatitis in mice. *Am J Pathol*, *177*(2), 713-723. https://doi.org/10.2353/ajpath.2010.091198

Wang, Q., Bode, A. M., & Zhang, T. (2023). Targeting CDK1 in cancer: mechanisms and implications. *npj Precision Oncology*, *7*(1), 58. https://doi.org/10.1038/s41698-023-00407-7

Wang, Y., Pan, W., Bai, X., Wang, X., Wang, Y., & Yin, Y. (2021). microRNA-454-mediated NEDD4-2/TrkA/cAMP axis in heart failure: Mechanisms and cardioprotective implications. *J Cell Mol Med*, *25*(11), 5082-5098. https://doi.org/10.1111/jcmm.16491

Wang, Z., Wu, L., Wang, H., Zhang, Y., & Xiao, H. (2022). Agonist-induced extracellular vesicles contribute to the transfer of functional bombesin receptor-subtype 3 to recipient cells. *Cellular and Molecular Life Sciences*, *79*(1). https://doi.org/10.1007/s00018-021-04114-z

Watts, V. J., Wiens, B. L., Cumbay, M. G., Vu, M. N., Neve, R. L., & Neve, K. A. (1998). Selective activation of Galphao by D2L dopamine receptors in NS20Y neuroblastoma cells. *J Neurosci*, *18*(21), 8692-8699. https://doi.org/10.1523/jneurosci.18-21-08692.1998

Welch, B. L. (1947). The generalisation of student's problems when several different population variances are involved. *Biometrika*, *34*(1-2), 28-35. https://doi.org/10.1093/biomet/34.1-2.28

Xu, Q., Wang, Y., Dabdoub, A., Smallwood, P. M., Williams, J., Woods, C., Kelley, M. W., Jiang, L., Tasman, W., Zhang, K., & Nathans, J. (2004). Vascular development in the retina and inner ear: control by Norrin and Frizzled-4, a high-affinity ligand-receptor pair. *Cell*, *116*(6), 883-895. https://doi.org/10.1016/s0092-8674(04)00216-8

Yang, W., Wang, J., Chen, Z., Chen, J., Meng, Y., Chen, L., Chang, Y., Geng, B., Sun, L., Dou, L., Li, J., Guan, Y., Cui, Q., & Yang, J. (2017). NFE2 Induces miR-423-5p to Promote Gluconeogenesis and Hyperglycemia by Repressing the Hepatic FAM3A-ATP-Akt Pathway. *Diabetes*, *66*(7), 1819-1832. https://doi.org/10.2337/db16-1172

Yang, Y. M., Lee, C. G., Koo, J. H., Kim, T. H., Lee, J. M., An, J., Kim, K. M., & Kim, S. G. (2015). Gα12 overexpressed in hepatocellular carcinoma reduces microRNA-122 expression via HNF4α inactivation, which causes c-Met induction. *Oncotarget*, *6*(22), 19055-19069. https://doi.org/10.18632/oncotarget.3957

Yoon, J. H., Jo, M. H., White, E. J., De, S., Hafner, M., Zucconi, B. E., Abdelmohsen, K., Martindale, J. L., Yang, X., Wood, W. H., 3rd, Shin, Y. M., Song, J. J., Tuschl, T., Becker, K. G., Wilson, G. M., Hohng, S., & Gorospe, M. (2015). AUF1 promotes let-7b loading on Argonaute 2. *Genes Dev*, *29*(15), 1599-1604. https://doi.org/10.1101/gad.263749.115

Zhang, C., Lai, M. B., Khandan, L., Lee, L. A., Chen, Z., & Junge, H. J. (2017). Norrin-induced Frizzled4 endocytosis and endo-lysosomal trafficking control retinal angiogenesis and barrier function. *Nature Communications*, *8*(1), 16050. https://doi.org/10.1038/ncomms16050

Zhang, H., Artiles, K. L., & Fire, A. Z. (2015). Functional relevance of "seed" and "non-seed" sequences in microRNA-mediated promotion of C. elegans developmental progression. *Rna*, *21*(11), 1980-1992. https://doi.org/10.1261/rna.053793.115

Zhang, L., Abedin, M., Jo, H.-N., Levey, J., Dinh, Q. C., Chen, Z., Angers, S., & Junge, H. J. (2023). A Frizzled4-LRP5 agonist promotes blood-retina barrier function by inducing a Norrin-like transcriptional response. *iScience*, *26*(8). https://doi.org/10.1016/j.isci.2023.107415

Zhang, Y., Xing, H., Guo, S., Zheng, Z., Wang, H., & Xu, D. (2016). MicroRNA-135b has a neuroprotective role via targeting of β-site APP-cleaving enzyme 1. *Exp Ther Med*, *12*(2), 809-814. https://doi.org/10.3892/etm.2016.3366

Zhang, Z., Lin, X., Wei, L., Wu, Y., Xu, L., Wu, L., Wei, X., Zhao, S., Zhu, X., & Xu, F. (2024). A framework for Frizzled-G protein coupling and implications to the PCP signaling pathways. *Cell Discov*, *10*(1), 3. https://doi.org/10.1038/s41421-023-00627-y

Zhao, L., Qian, X., Ren, Z., & Wang, A. (2024). miR-31-5p suppresses myocardial hypertrophy by targeting Nfatc2ip. *J Cell Mol Med*, *28*(12), e18413. https://doi.org/10.1111/jcmm.18413

15. FIGURES AND TABLES

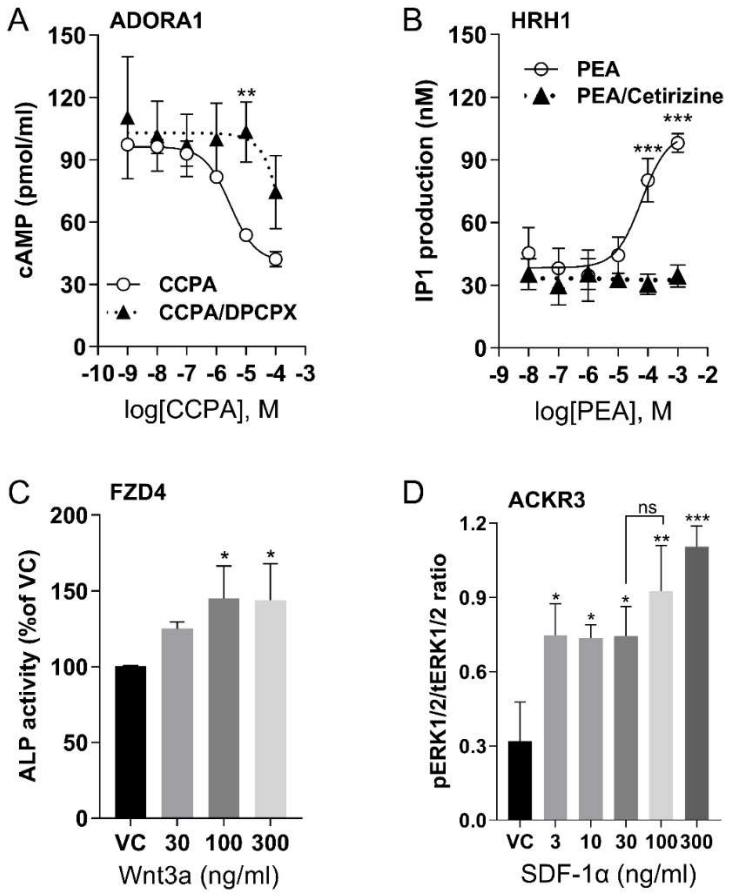

Figure 1. GPCR activation in U2OS cells by selective agonists

(**A**) Dose-dependent cAMP accumulation after ADORA1 activation with agonist, CCPA, or inhibition with antagonist DPCPX (5μM). (**B**) Dose-dependent IP1 accumulation after PEA stimulation of HRH1 and inhibition by Cetirizine (1μM). (**C**) ALP activity after stimulation of FZD4 by Wnt3a. (**D**) The ratio of phosphorylated ERK1/2 (pERK1/2) by total ERK 1/2 (tERK1/2) after stimulation of ACKR3 by SDF-1α. For all graphs, data are shown as mean ± SD, with n=3 independent repeats, each having duplicate determinants, ns=not significant, *$p < 0.05$, **$p < 0.01$, ***$p < 0.001$ vs vehicle control (VC). Statistical significances were determined by one way or two-way ANOVA of receptors by agonists or antagonists and post-hoc Tukey or Sidak testing for multiple comparisons.

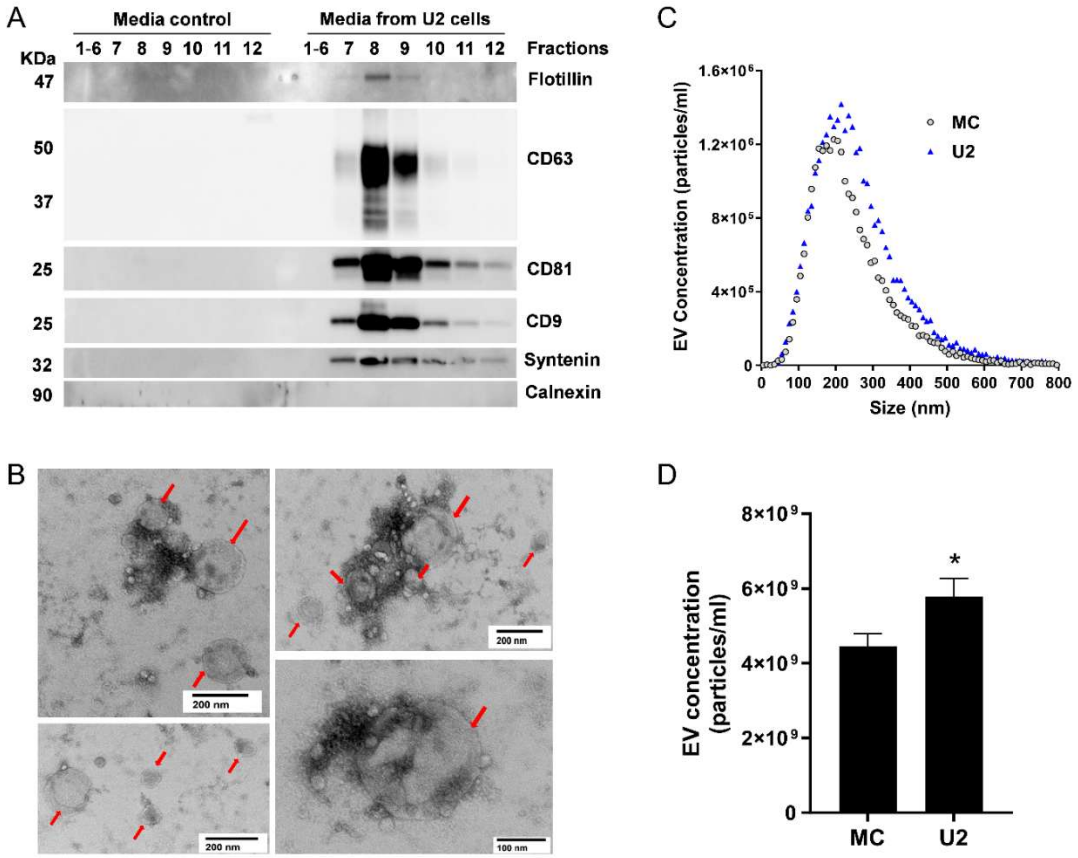

Figure 2. Characterization of EVs isolated from U2OS cell culture media

(**A**) Representative immunoblots of EVs isolated by SEC from U2OS cell culture media (U2) but not from media control (MC) show detection of EV markers including CD9, CD63, CD81, flotillin, and syntenin, in EV fractions 7-9. Endoplasmic reticulum marker, calnexin, was not detected in the EV fractions. (**B**) Representative images from transmission electron microscopy of isolated EVs (red arrows) from pooled EV-enriched fractions 7-9. (**C**) Size distribution of pooled EV fractions 7-9 isolated from MC and U2. (**D**) Quantification of pooled EV fractions 7-9 of MC and U2 measured by f-NTA. Data are shown as mean ± SEM, n=7-8. A Student's *t*-test determined significant differences in the EV concentration between the MC and U2, $*p < 0.05$.

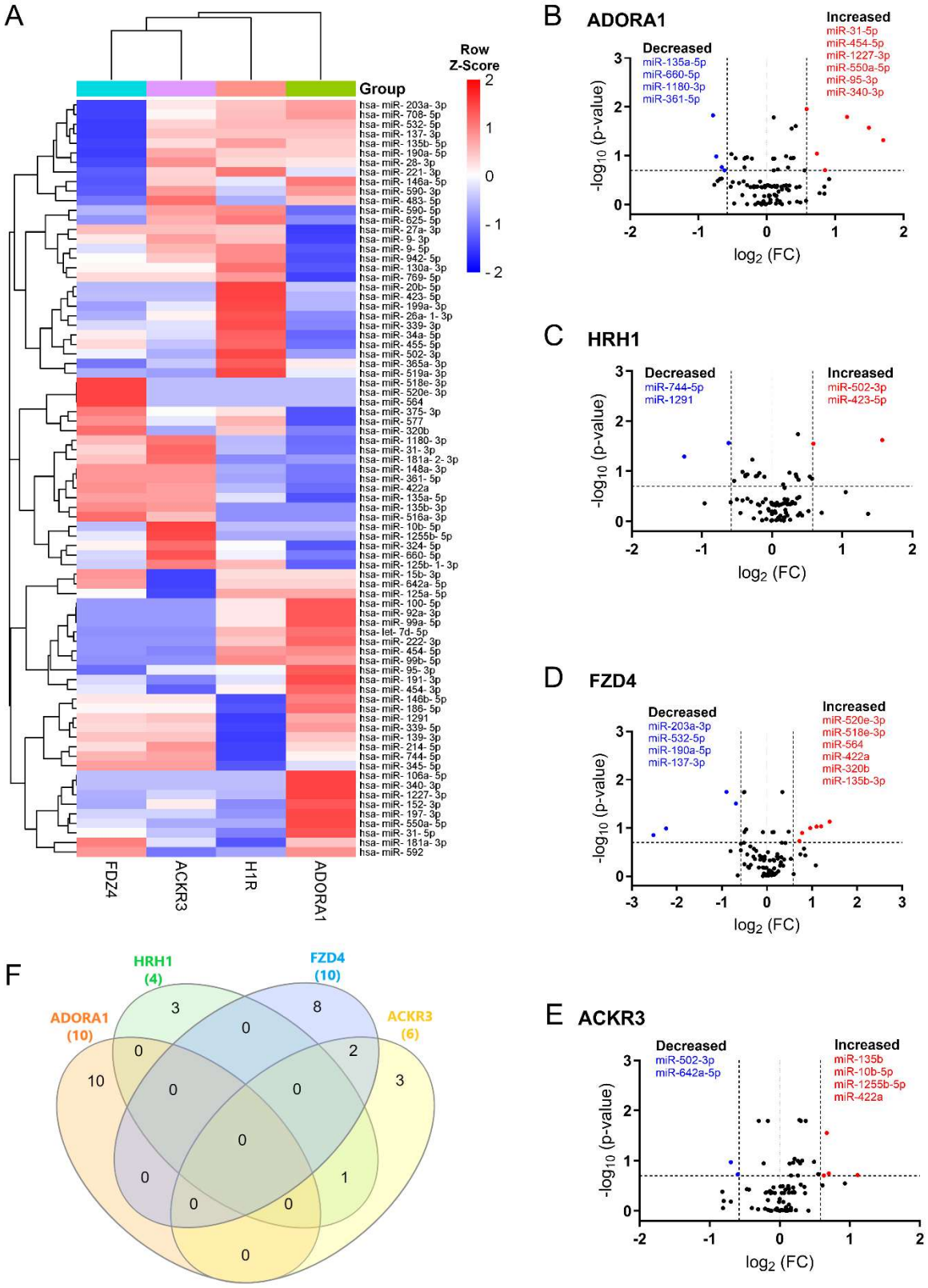
A
Row Z-Score
2
1
0
- 1
- 2
Group
hsa- miR- 203a- 3p
hsa- miR- 708- 5p
hsa- miR- 532- 5p
hsa- miR- 137- 3p
hsa- miR- 135b- 5p
hsa- miR- 190a- 5p
hsa- miR- 28- 3p
hsa- miR- 221- 3p
hsa- miR- 146a- 5p
hsa- miR- 590- 3p
hsa- miR- 483- 5p
hsa- miR- 590- 5p
hsa- miR- 625- 5p
hsa- miR- 27a- 3p
hsa- miR- 9- 3p
hsa- miR- 9- 5p
hsa- miR- 942- 5p
hsa- miR- 130a- 3p
hsa- miR- 769- 5p
hsa- miR- 20b- 5p
hsa- miR- 423- 5p
hsa- miR- 199a- 3p
hsa- miR- 28a- 1- 3p
hsa- miR- 339- 3p
hsa- miR- 34a- 5p
hsa- miR- 455- 5p
hsa- miR- 502- 3p
hsa- miR- 365a- 3p
hsa- miR- 519a- 3p
hsa- miR- 518e- 3p
hsa- miR- 520e- 3p
hsa- miR- 564
hsa- miR- 375- 3p
hsa- miR- 577
hsa- miR- 320b
hsa- miR- 1180- 3p
hsa- miR- 31- 3p
hsa- miR- 181a- 2- 3p
hsa- miR- 148a- 3p
hsa- miR- 361- 5p
hsa- miR- 422a
hsa- miR- 135a- 5p
hsa- miR- 135b- 3p
hsa- miR- 516a- 3p
hsa- miR- 10b- 5p
hsa- miR- 1255b- 5p
hsa- miR- 324- 5p
hsa- miR- 660- 5p
hsa- miR- 125b- 1- 3p
hsa- miR- 15b- 3p
hsa- miR- 642a- 5p
hsa- miR- 125a- 5p
hsa- miR- 100- 5p
hsa- miR- 92a- 3p
hsa- miR- 99a- 5p
hsa- let- 7d- 5p
hsa- miR- 222- 3p
hsa- miR- 454- 5p
hsa- miR- 99b- 5p
hsa- miR- 95- 3p
hsa- miR- 191- 3p
hsa- miR- 454- 3p
hsa- miR- 146b- 5p
hsa- miR- 186- 5p
hsa- miR- 1291
hsa- miR- 339- 5p
hsa- miR- 139- 3p
hsa- miR- 214- 5p
hsa- miR- 744- 5p
hsa- miR- 345- 5p
hsa- miR- 106a- 5p
hsa- miR- 340- 3p
hsa- miR- 1227- 3p
hsa- miR- 152- 3p
hsa- miR- 197- 3p
hsa- miR- 550a- 5p
hsa- miR- 31- 5p
hsa- miR- 181a- 3p
hsa- miR- 592
FDZ4
ACKR3
H1R
ADORA1
B
ADORA1
Decreased
miR-135a-5p
miR-660-5p
miR-1180-3p
miR-361-5p
Increased
miR-31-5p
miR-454-5p
miR-1227-3p
miR-550a-5p
miR-95-3p
miR-340-3p
-log10 (p-value)
log2 (FC)
C
HRH1
Decreased
miR-744-5p
miR-1291
Increased
miR-502-3p
miR-423-5p
-log10 (p-value)
log2 (FC)
D
FZD4
Decreased
miR-203a-3p
miR-532-5p
miR-190a-5p
miR-137-3p
Increased
miR-520e-3p
miR-518e-3p
miR-564
miR-422a
miR-320b
miR-135b-3p
-log10 (p-value)
log2 (FC)
E
ACKR3
Decreased
miR-502-3p
miR-642a-5p
Increased
miR-135b
miR-10b-5p
miR-1255b-5p
miR-422a
-log10 (p-value)
log2 (FC)
F
HRH1 (4)
FZD4 (10)
ADORA1 (10)
ACKR3 (6)

Figure 3. Differentially expressed EV miRNAs in response to GPCR activation

(**A**) The heatmap showed unsupervised hierarchical clustering of miRNA expression (row) following GPCR stimulation (column). The relative abundance of miRNAs is represented in Z-score value (z-transformed fold changes), blue, below-mean expression; red, above-mean expression. (**B-E**) Volcano plots displayed the analysis of EV miRNAs after ADORA1 (**B**), HRH1 (**C**), FZD4 (**D**), and ACKR3 (**E**) activation. On the x-axis, the dotted line indicates miRNAs that satisfied the $|\log_2 \text{fold change}| \geq 1.5$ cut-off, while the dotted line on the y-axis indicates miRNA that met Skillings-Mack p-value < 0.2. (**F**) Venn diagram showed the miRNAs of interest with at least 1.5-fold change across four GPCR groups following treatment. n=5-6 replicates per GPCR group.

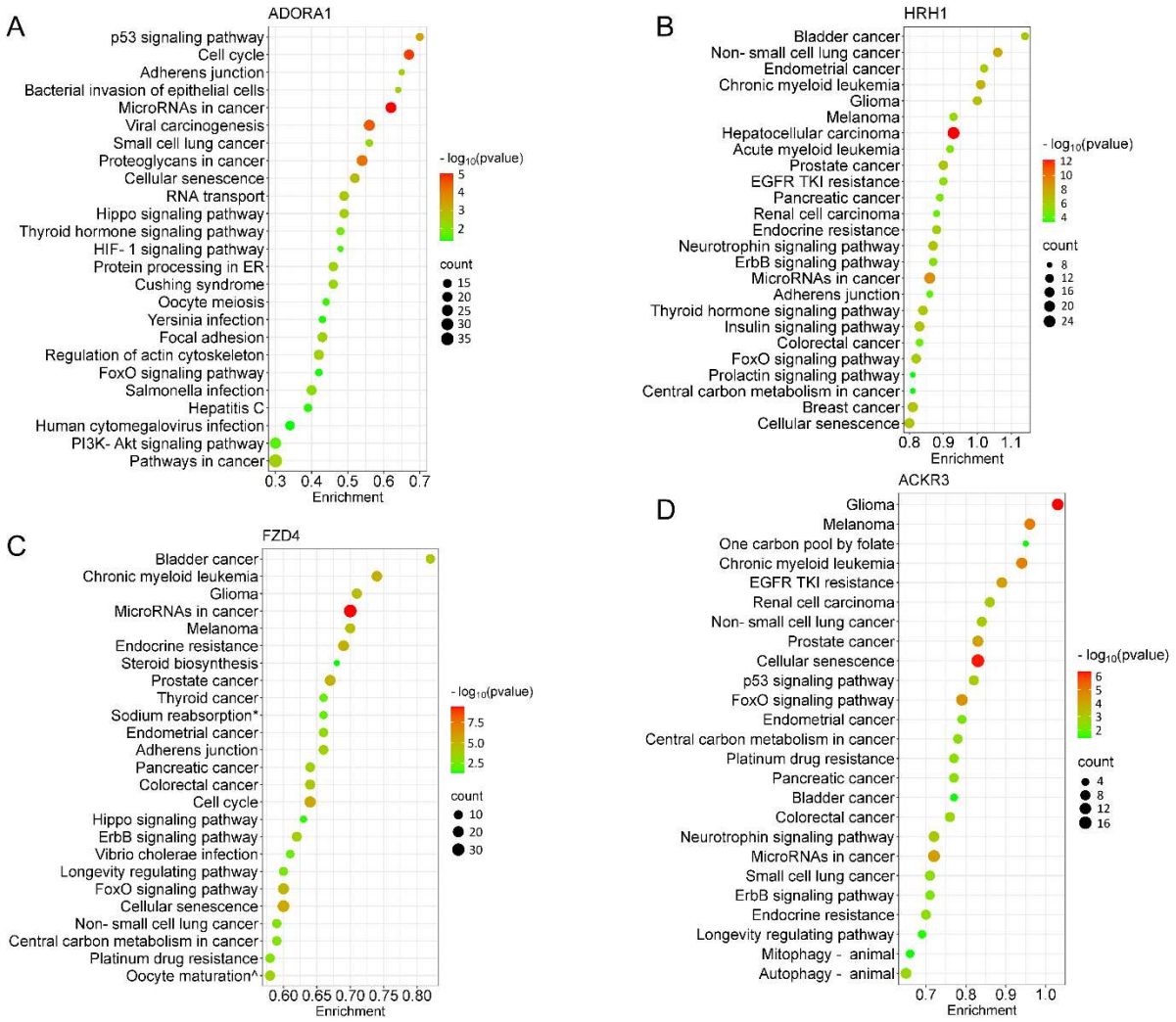

Figure 4. Pathway analysis of the differentially expressed EV miRNA after GPCR activation

The bubble plots showed the top 25 significantly enriched KEGG pathways for the miRNAs (≥ 1.5-fold change) of individual GPCR. (**A**) ADORA1, (**B**) HRH1, (**C**) FZD4, (**D**) ACKR3. The dot size represents the number of enriched gene targets, and the color shows the *p*-value of the enrichment. For the enrichment analysis, cut-off criteria were *p*-value (FDR) < 0.05 and gene count > 2. KEGG terms: * Endocrine and other factor-regulated calcium reabsorption, ^ Progesterone-mediated oocyte maturation.

GPCRs	miRNAs	log_2 (FC)	*p* value	SD of log_2(FC)
ADORA1	hsa-miR-550a-5p	1.70	0.0455	0.22
	hsa-miR-1227-3p	1.49	0.0253	0.16
	hsa-miR-454-5p	1.17	0.0143	0.27
	hsa-miR-31-5p	0.58	0.0143	0.07
	hsa-miR-135a-5p	-0.79	0.0143	0.18
HRH1	hsa-miR-502-3p	1.57	0.025	0.26
	hsa-miR-423-5p	0.59	0.025	0.16
	hsa-miR-744-5p	-0.62	0.025	0.14
FZD4	hsa-miR-203a-3p	-0.90	0.0143	0.16
ACKR3	hsa-miR-135b-3p	0.67	0.0253	0.11

Table 1. EV miRNAs differentially expressed in 4 GPCR groups.

Differentially expressed miRNAs ($p < 0.05$) were identified in each treatment group compared to its vehicle control, n=5-6 samples of each group.

Supplemental Materials

Figure S1. Sensitivity analysis across alternative estimates of treatment effects. (**A**) Scatterplot matrix showing pairwise concordance of alternative treatment-effect estimators, including all per-miRNA estimates from all receptors combined, with text labels (in quotes) indexed to the table below; note that the perfect correlation in the "individual" and "matched" approaches is expected, and the "pooled" and "batched" approaches only apply to the receptors ADORA1 and H1R. All estimators not based on matched pairs demonstrate bias in the form of exaggeration of effect size on average, and estimators employing a higher degree of aggregation (either at the treatment group or batch level) show worse correlation with the unbiased matched-pairs estimator (an example of ecological bias); it is clear that process variance brings considerable risk of bias in experiments of this type, and that great care should be taken to provide adequate representation of process variance via controls across experiments. (**B**) Comparison table detailing the differences between alternative estimators, including advantages and disadvantages of each approach. Our preferred approach is "matched", on both theoretical and empirical grounds. Briefly, the six combinations were: 1) treatment effect estimated as difference of group medians with permutation-based p-value; 2) difference of group medians with p-value from Welch's robust t-test; 3) (applies to batched receptors only) treatment coefficient from median regression of pooled-batch data with p-value from the rank-based Mann-Whitney test; 4) (applies to batched receptors only) sample-weighted average of treatment coefficients from separate median regressions of data from each batch with p-value as the harmonic mean of Mann-Whitney p-values calculated separately on each batch; 5) mean matched-pairs estimator (simple average of all within-pair differences between agonist and vehicle control) with permutation-based p-value; and 6) regression matched-pairs estimator (treatment coefficient from a within-pairs linear regression) with p-value from the unbalanced-robust rank-based Skillings-Mack test. Note that (1) was the only approach where we applied group-based normalization (for all others we used run-based), and that the treatment effects in (5) and (6) are not strictly the same except in the absence of missing data but they are operationally 100% correlated.

Table S1. The analysis of GPCR gene expression across various cell lines, as sourced from the Human Protein Atlas.

Figure S2. Representative immunoblots showed stimulation of ACKR3 with SDF-1α-induced phosphorylation of ERK1/2 (pERK1/2) compared to total ERK1/2 (tERK1/2). β-actin was used as a loading control.

Figure S3. Quantification of EVs in U2OS media in response to receptor activation. U2OS cells were incubated with vehicle control (VC) or a selective agonist CCPA (**A**), PEA (**B**), Wnt3a (**C**), or SDF-1α (**D**) for ADORA1, HRH1, FZD4, and ACKR3, respectively. EVs were isolated and the concentration was normalized as a percentage of the media control (MC). EV size distribution following agonist or VC treatment in ADORA1 (**E**), HRH1 (**F**), FZD4 (**G**), and ACKR3 (**H**). Data are shown as mean ± SEM, n=3. A t-test determined no significant differences in EV concentration or size distribution between the VC and agonist stimulation in all GPCRs, $p > 0.05$.

Table S2. miRNAs detected in media control.

Table S3. Differentially expressed miRNAs in the isolated EVs following GPCR activation. All differentially expressed miRNAs (meeting $p < 0.2$) after stimulation were listed.

Figure S4. The top 10 hub genes identified in miRNA targets (≥ 1.5-fold change) PPI network.

Figure S5. Pathway analysis of miR-502-3p and miR-137 targets.

The bubble plots showed the top 25 significantly enriched KEGG pathways for the targets of (**A**) miR-502-3p and (**B**) miR-137. The dot size represents the number of enriched gene targets, and the color shows the *p*-value of the enrichment. For the enrichment analysis, the cut-off criteria were *p*-value (FDR) < 0.05 and gene count > 2. KEGG term abbreviations: ** Aldosterone-regulated sodium reabsorption.

SUPPLEMENTARY FIGURES AND TABLES

Figure S1

A

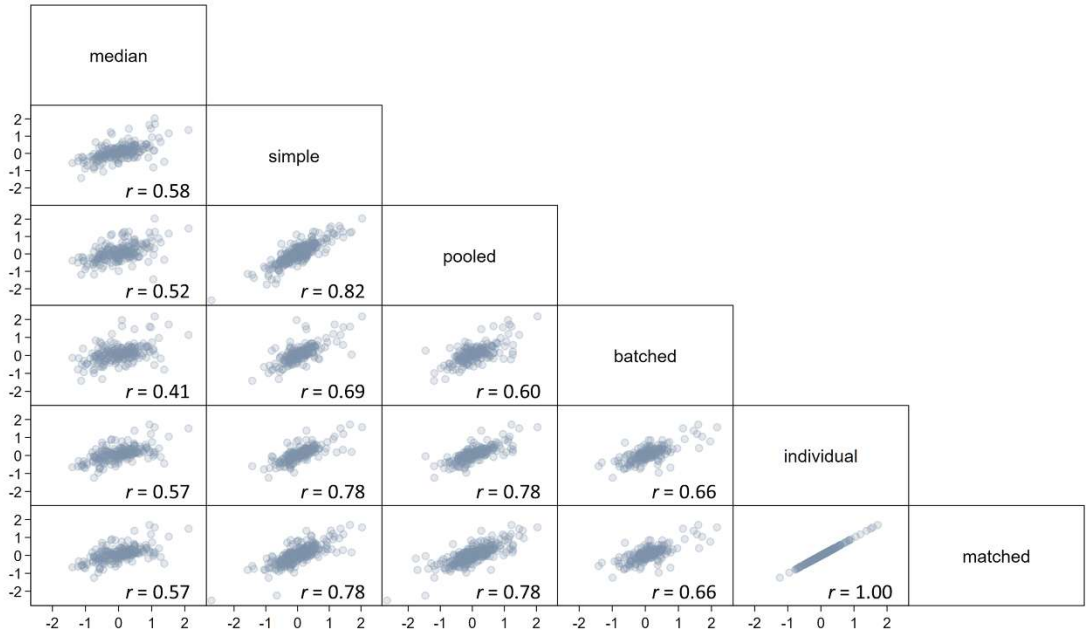

B

Method	Normalization	Effect estimate	P-value	PROS	CONS
Group medians (original = "median")	Align group medians	$Median_1 - Median_0$	Permutation test	Easy to do	Retains within-group technical variance
Group medians (new = "simple")	Align run medians	$Median_1 - Median_0$	Robust t-test	Easy to do	P-value sensitive to outlier observations
Pooled-batches ("pooled")	Align run medians	β_{TX} coefficient from median regression	Mann-Whitney test	Accurate p-value	Ignores batch differences in treatment effects
Batch-averaged ("batched")	Align run medians	Weighted average of the β_{TX1} and β_{TX2} coefficients from batch-specific median regressions	Harmonic mean of the p-values from batch-specific Mann-Whitney tests	Accounts for batch differences in treatment effects	Low power, sensitive to batch differences in missingness
Matched-pairs (mean = "individual")	Align run medians	Simple average of all pair-specific TX − VC differences	Permutation test	Accounts for any correlation of process order with treatment effects (stronger than a batch correction!)	P-value sensitive to process order of missing pairs
Matched-pairs (regression = "matched")	Align run medians	β_{TX} coefficient from within-pairs (aka FE) linear regression	Skillings-Mack test	Accurate p-value	NONE

Table S1

Cell line	Gene	Gene description	UniProt evidence
SH-SY5Y	GRM7	Glutamate metabotropic receptor 7	Evidence at protein level
	ADCYAP1R1	ADCYAP receptor type I	Evidence at protein level
	ADGRA2	Adhesion G protein-coupled receptor A2	Evidence at protein level
	ADGRL2	Adhesion G protein-coupled receptor L2	Evidence at protein level
	PTGDR	Prostaglandin D2 receptor	Evidence at transcript level
	VN1R1	Vomeronasal 1 receptor 1	Evidence at transcript level
A-431	ADGRG2	Adhesion G protein-coupled receptor G2	Evidence at protein level
	ADORA2B	Adenosine A2b receptor	Evidence at protein level
	ADRB2	Adrenoceptor beta 2	Evidence at protein level
	CELSR2	Cadherin EGF LAG seven-pass G-type receptor 2	Evidence at protein level
	EDNRB	Endothelin receptor type B	Evidence at protein level
	FZD3	Frizzled class receptor 3	Evidence at protein level
	FZD6	Frizzled class receptor 6	Evidence at protein level
	GPR87	G protein-coupled receptor 87	Evidence at transcript level
	GRM1	Glutamate metabotropic receptor 1	Evidence at protein level
	OR10Q1	Olfactory receptor family 10 subfamily Q member 1	Evidence at transcript level
	P2RY2	Purinergic receptor P2Y2	Evidence at protein level
	SSTR2	Somatostatin receptor 2	Evidence at protein level
	TACR2	Tachykinin receptor 2	Evidence at protein level
U-251MG	HTR7	5-hydroxytryptamine receptor 7	Evidence at protein level
	S1PR1	Sphingosine-1-phosphate receptor 1	Evidence at protein level
	ADRA1B	Adrenoceptor alpha 1B	Evidence at protein level
	CCR4	C-C motif chemokine receptor 4	Evidence at protein level
	EDNRA	Endothelin receptor type A	Evidence at protein level
	FZD1	Frizzled class receptor 1	Evidence at protein level
	GPR142	G protein-coupled receptor 142	Evidence at transcript level
	GPRC5B	G protein-coupled receptor class C group 5 member B	Evidence at transcript level
	LGR6	Leucine rich repeat containing G protein-coupled receptor 6	Evidence at protein level
	MAS1L	MAS1 proto-oncogene like, G protein-coupled receptor	Evidence at transcript level
	OR6P1	Olfactory receptor family 6 subfamily P member 1	No human protein/transcript evidence
	PTAFR	Platelet activating factor receptor	Evidence at protein level
U2OS	GPRC5A	G protein-coupled receptor class C group 5 member A	Evidence at protein level
	GLP2R	Glucagon like peptide 2 receptor	Evidence at protein level
	NMBR	Neuromedin B receptor	Evidence at protein level
	OR4N4	Olfactory receptor family 4 subfamily N member 4	Evidence at transcript level
	ACKR2	Atypical chemokine receptor 2	Evidence at protein level
	ACKR3	Atypical chemokine receptor 3	Evidence at protein level
	ADGRE5	Adhesion G protein-coupled receptor E5	Evidence at protein level
	ADGRF4	Adhesion G protein-coupled receptor F4	Evidence at protein level
	ADORA1	Adenosine A1 receptor	Evidence at protein level
	CALCRL	Calcitonin receptor like receptor	Evidence at protein level

	CCR7	C-C motif chemokine receptor 7	Evidence at protein level
	CRHR2	Corticotropin releasing hormone receptor 2	Evidence at protein level
	DRD4	Dopamine receptor D4	Evidence at protein level
	F2RL1	F2R like trypsin receptor 1	Evidence at protein level
	FZD4	Frizzled class receptor 4	Evidence at protein level
	FZD8	Frizzled class receptor 8	Evidence at protein level
	GABBR1	Gamma-aminobutyric acid type B receptor subunit 1	Evidence at protein level
	GCGR	Glucagon receptor	Evidence at protein level
	GPR156	G protein-coupled receptor 156	Evidence at transcript level
	GPR162	G protein-coupled receptor 162	Evidence at protein level
	GPR17	G protein-coupled receptor 17	Evidence at protein level
	GPR173	G protein-coupled receptor 173	Evidence at protein level
	GPR27	G protein-coupled receptor 27	Evidence at transcript level
	GPR34	G protein-coupled receptor 34	Evidence at transcript level
	GPR63	G protein-coupled receptor 63	Evidence at transcript level
	HRH1	Histamine receptor H1	Evidence at protein level
	NPFFR2	Neuropeptide FF receptor 2	Evidence at protein level
	S1PR4	Sphingosine-1-phosphate receptor 4	Evidence at protein level
	SSTR3	Somatostatin receptor 3	Evidence at protein level
	VIPR2	Vasoactive intestinal peptide receptor 2	Evidence at protein level

Figure S2

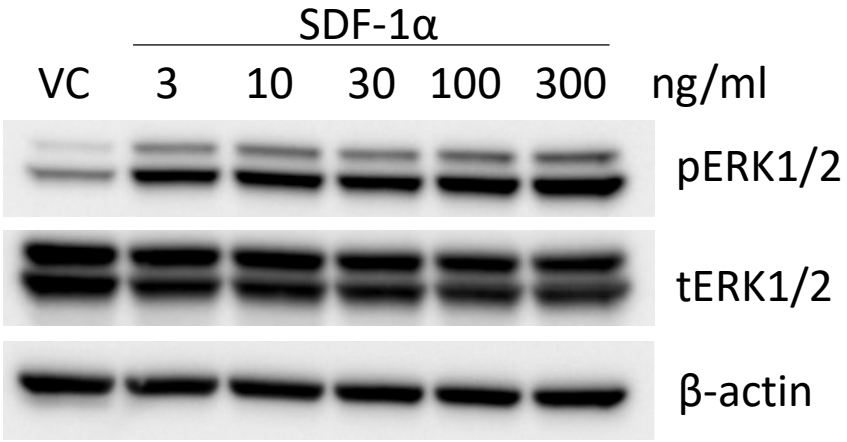

Figure S3

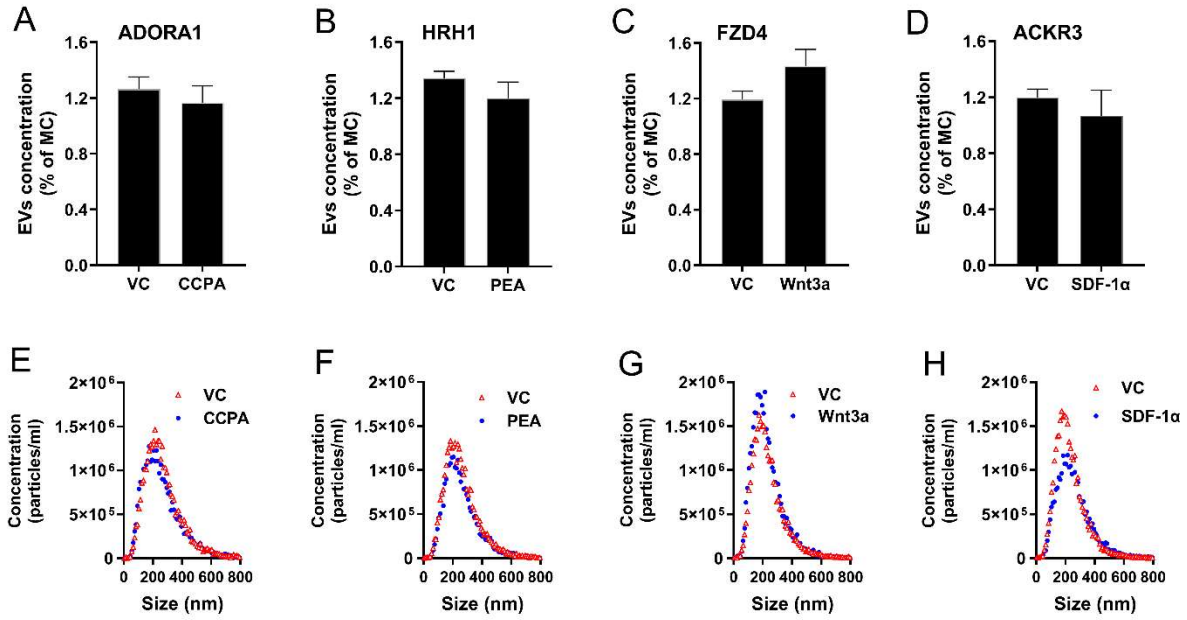
A
ADORA1
EVs concentration (% of MC)
1.6
1.2
0.8
0.4
0.0
VC
CCPA
B
HRH1
Evs concentration (% of MC)
VC
PEA
C
FZD4
EVs concentration (% of MC)
VC
Wnt3a
D
ACKR3
EVs concentration (% of MC)
VC
SDF-1α
E
Concentration (particles/ml)
2×10⁶
1.5×10⁶
1×10⁶
5×10⁵
0
VC
CCPA
0 200 400 600 800
Size (nm)
F
Concentration (particles/ml)
VC
PEA
Size (nm)
G
Concentration (particles/ml)
VC
Wnt3a
Size (nm)
H
Concentration (particles/ml)
VC
SDF-1α
Size (nm)

Table S2

miRNA	Average Ct	SD
hsa-miR-106b-5p	25.7	1.4
hsa-miR-126-5p	27.0	0.8
hsa-miR-126-3p	24.6	1.1
hsa-miR-127-3p	26.4	0.7
hsa-miR-1305	30.4	0.2
hsa-miR-142-3p	26.4	1.6
hsa-miR-150-5p	26.4	0.6
hsa-miR-15b-5p	27.8	1.0
hsa-miR-192-5p	28.5	0.8
hsa-miR-194-5p	29.6	0.3
hsa-miR-204-5p	28.8	0.5
hsa-miR-215-5p	29.0	0.6
hsa-miR-223-3p	23.1	0.9
hsa-miR-25-3p	28.0	0.8
hsa-miR-26a-5p	26.1	0.8
hsa-miR-26b-5p	29.1	1.0
hsa-miR-27b-3p	30.1	0.2
hsa-miR-30b-5p	25.0	0.8
hsa-miR-30c-5p	25.0	1.2
hsa-miR-331-3p	25.6	0.8
hsa-miR-338-5p	24.5	0.1
hsa-miR-376a-3p	28.7	0.5
hsa-miR-378	28.8	2.6
hsa-miR-409-3p	26.9	1.3
hsa-miR-494-3p	28.5	0.9
hsa-miR-505-5p	32.3	0.8
hsa-miR-520c-3p	26.3	0.2
hsa-miR-520d-3p	25.8	0.9
hsa-miR-539-5p	29.2	1.2
hsa-miR-548a-3p	30.6	0.4
hsa-miR-572	26.7	0.3
hsa-miR-601	29.2	0.6
hsa-miR-625-3p	28.1	0.2
hsa-miR-628-5p	31.1	0.6
hsa-miR-875-5p	32.3	0.5
hsa-miR-451a	24.3	1.2

Table S3

miRNA	Log_2 fold change	*p* value
Adenosine A1 receptor (ADORA1)		
miR-550a-5p	1.7	0.0455
miR-1227-3p	1.49	0.0253
miR-454-5p	1.17	0.0143
miR-340-3p	0.85	0.1797
miR-95-3p	0.73	0.1024
miR-31-5p	0.58	0.0143
miR-592	0.55	0.1797
miR-100-5p	0.42	0.0253
let-7d-5p	0.39	0.1024
miR-99a-5p	0.36	0.0253
miR-454-3p	0.35	0.1024
miR-99b-5p	0.31	0.1797
miR-708-5p	0.28	0.1024
miR-1291	0.16	0.1797
miR-92a-3p	0.11	0.1024
miR-186-5p	0.1	0.0143
miR-106a-5p	0.1	0.1797
miR-135b-5p	0.09	0.1024
miR-27a-3p	-0.22	0.1024
miR-339-3p	-0.29	0.1024
miR-942-5p	-0.32	0.1024
miR-148a-3p	-0.33	0.1024
miR-577	-0.33	0.1797
miR-130a-3p	-0.46	0.1024
miR-769-5p	-0.52	0.1024
miR-361-5p	-0.62	0.1797
miR-1180-3p	-0.66	0.1797
miR-660-5p	-0.74	0.1024
miR-135a-5p	-0.79	0.0143
Histamine receptor H1 (HRH1)		
miR-502-3p	1.57	0.0253
miR-423-5p	0.59	0.0253
miR-34a-5p	0.57	0.1797
miR-365a-3p	0.54	0.1024
miR-519a-3p	0.38	0.1797
miR-199a-3p	0.37	0.0143
miR-130a-3p	0.35	0.1024
miR-99b-5p	0.34	0.1024
miR-708-5p	0.25	0.1024
miR-20b-5p	0.18	0.1797
miR-222-3p	0.16	0.1797
miR-197-3p	-0.11	0.1024

miR-181a-2-3p	-0.18	0.1024
miR-146a-5p	-0.21	0.1024
miR-146b-5p	-0.23	0.1024
miR-139-3p	-0.28	0.0455
miR-483-5p	-0.35	0.1024
miR-214-5p	-0.38	0.1024
miR-345-5p	-0.38	0.1024
miR-1180-3p	-0.42	0.1024
miR-339-5p	-0.54	0.1797
miR-744-5p	-0.62	0.0253
miR-1291	-1.25	0.1024
Frizzled class receptor 4 (FZD4)		
miR-518e-3p	1.39	0.0833
miR-422a	1.2	0.1024
miR-564	1.1	0.0833
miR-520e-3p	0.96	0.0833
miR-320b	0.78	0.1024
miR-135b-3p	0.72	0.1797
miR-375-3p	0.48	0.1024
miR-181a-3p	0.41	0.1797
miR-577	0.34	0.0143
miR-1227-3p	0.33	0.1797
miR-15b-3p	0.15	0.1024
miR-455-5p	0.15	0.1024
miR-28-3p	-0.09	0.1024
miR-483-5p	-0.46	0.1024
miR-95-3p	-0.5	0.0143
miR-590-3p	-0.5	0.1024
miR-660-5p	-0.51	0.0143
miR-625-5p	-0.51	0.1797
miR-532-5p	-0.69	0.1024
miR-203a-3p	-0.9	0.0143
miR-190a-5p	-2.24	0.0833
miR-137-3p	-2.52	0.1797
Atypical chemokine receptor 3 (ACKR3)		
miR-422a	1.11	0.1797
miR-1255b-5p	0.7	0.1797
miR-135b-3p	0.67	0.0253
miR-10b-5p	0.63	0.1797
miR-516a-3p	0.55	0.1797
miR-1227-3p	0.49	0.1024
miR-9-3p	0.37	0.0143
miR-9-5p	0.32	0.1024
miR-324-5p	0.3	0.0143
miR-26a-1-3p	0.29	0.1024
miR-152-3p	0.28	0.0143
miR-221-3p	0.26	0.1797
miR-31-3p	0.26	0.1024

miR-1180-3p	0.21	0.0833
miR-708-5p	0.19	0.1024
miR-125b-1-3p	0.16	0.1797
miR-590-5p	0.14	0.1024
miR-339-3p	-0.17	0.0143
miR-191-3p	-0.23	0.1024
miR-125a-5p	-0.3	0.0143
miR-502-3p	-0.6	0.1797
miR-642a-5p	-0.7	0.1024

Figure S4

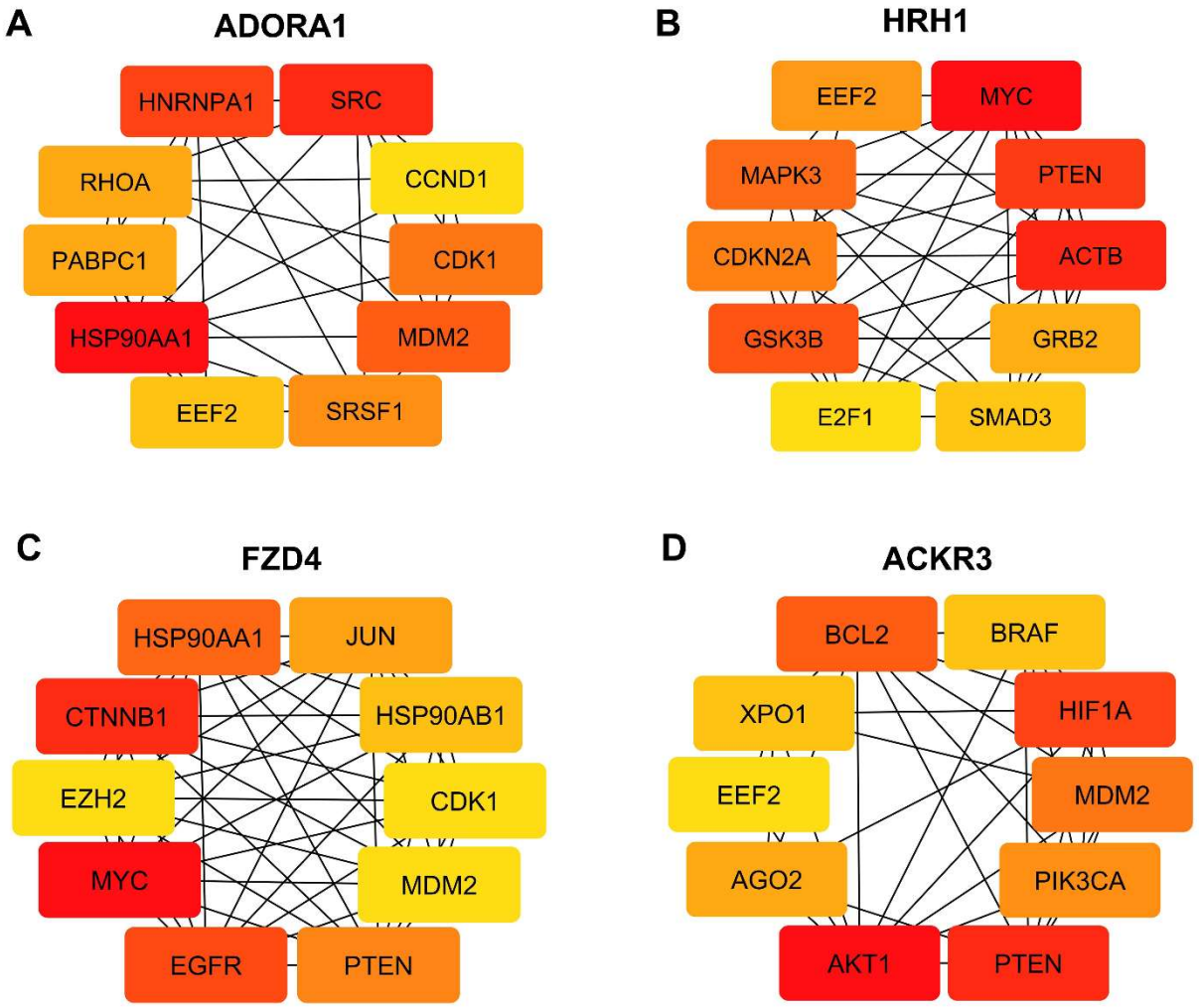
A
ADORA1
HNRNPA1
SRC
RHOA
CCND1
PABPC1
CDK1
HSP90AA1
MDM2
EEF2
SRSF1
B
HRH1
EEF2
MYC
MAPK3
PTEN
CDKN2A
ACTB
GSK3B
GRB2
E2F1
SMAD3
C
FZD4
HSP90AA1
JUN
CTNNB1
HSP90AB1
EZH2
CDK1
MYC
MDM2
EGFR
PTEN
D
ACKR3
BCL2
BRAF
XPO1
HIF1A
EEF2
MDM2
AGO2
PIK3CA
AKT1
PTEN

Figure S5

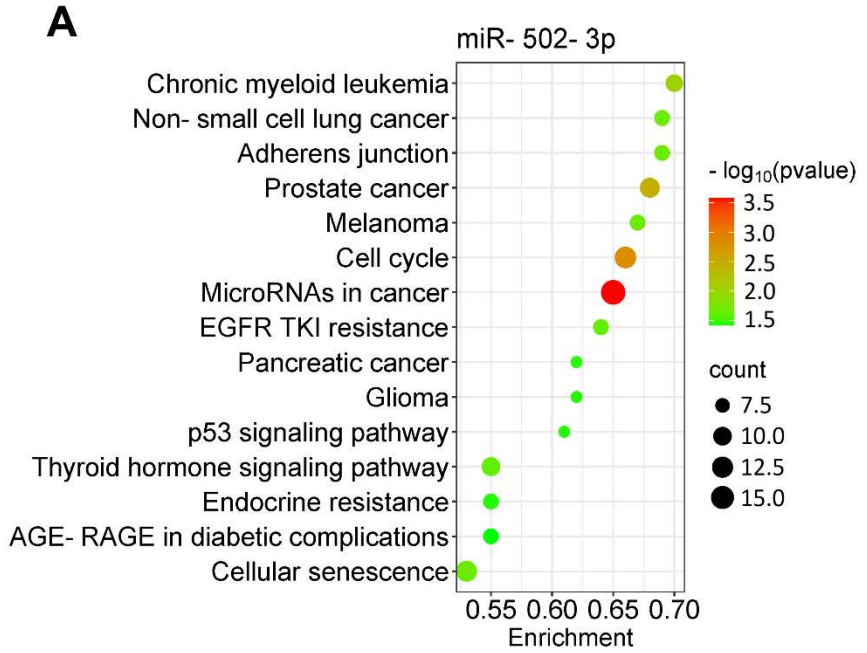
A
miR- 502- 3p
Chronic myeloid leukemia
Non- small cell lung cancer
Adherens junction
Prostate cancer
Melanoma
Cell cycle
MicroRNAs in cancer
EGFR TKI resistance
Pancreatic cancer
Glioma
p53 signaling pathway
Thyroid hormone signaling pathway
Endocrine resistance
AGE- RAGE in diabetic complications
Cellular senescence
0.55 0.60 0.65 0.70
Enrichment
- log10(pvalue)
3.5
3.0
2.5
2.0
1.5
count
7.5
10.0
12.5
15.0

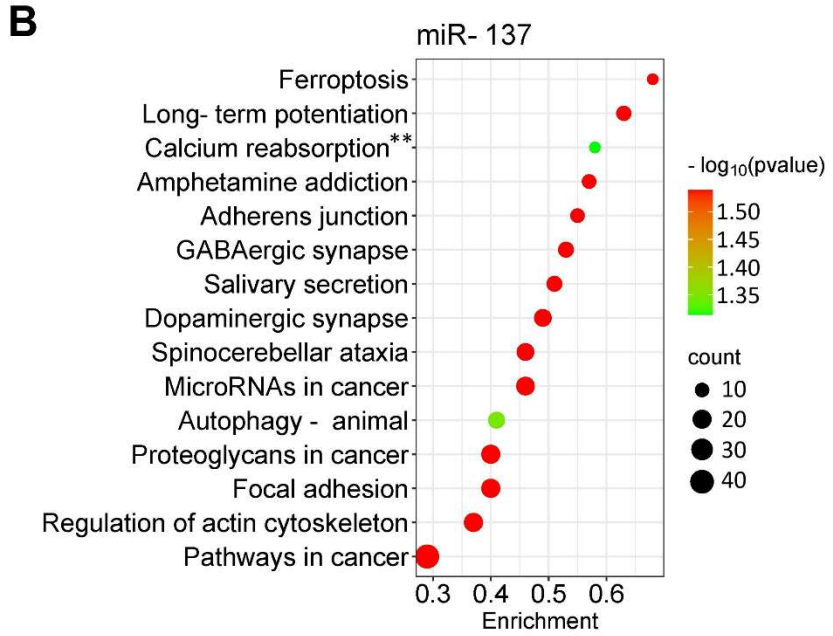
B
miR- 137
Ferroptosis
Long- term potentiation
Calcium reabsorption**
Amphetamine addiction
Adherens junction
GABAergic synapse
Salivary secretion
Dopaminergic synapse
Spinocerebellar ataxia
MicroRNAs in cancer
Autophagy - animal
Proteoglycans in cancer
Focal adhesion
Regulation of actin cytoskeleton
Pathways in cancer
0.3 0.4 0.5 0.6
Enrichment
- log10(pvalue)
1.50
1.45
1.40
1.35
count
10
20
30
40
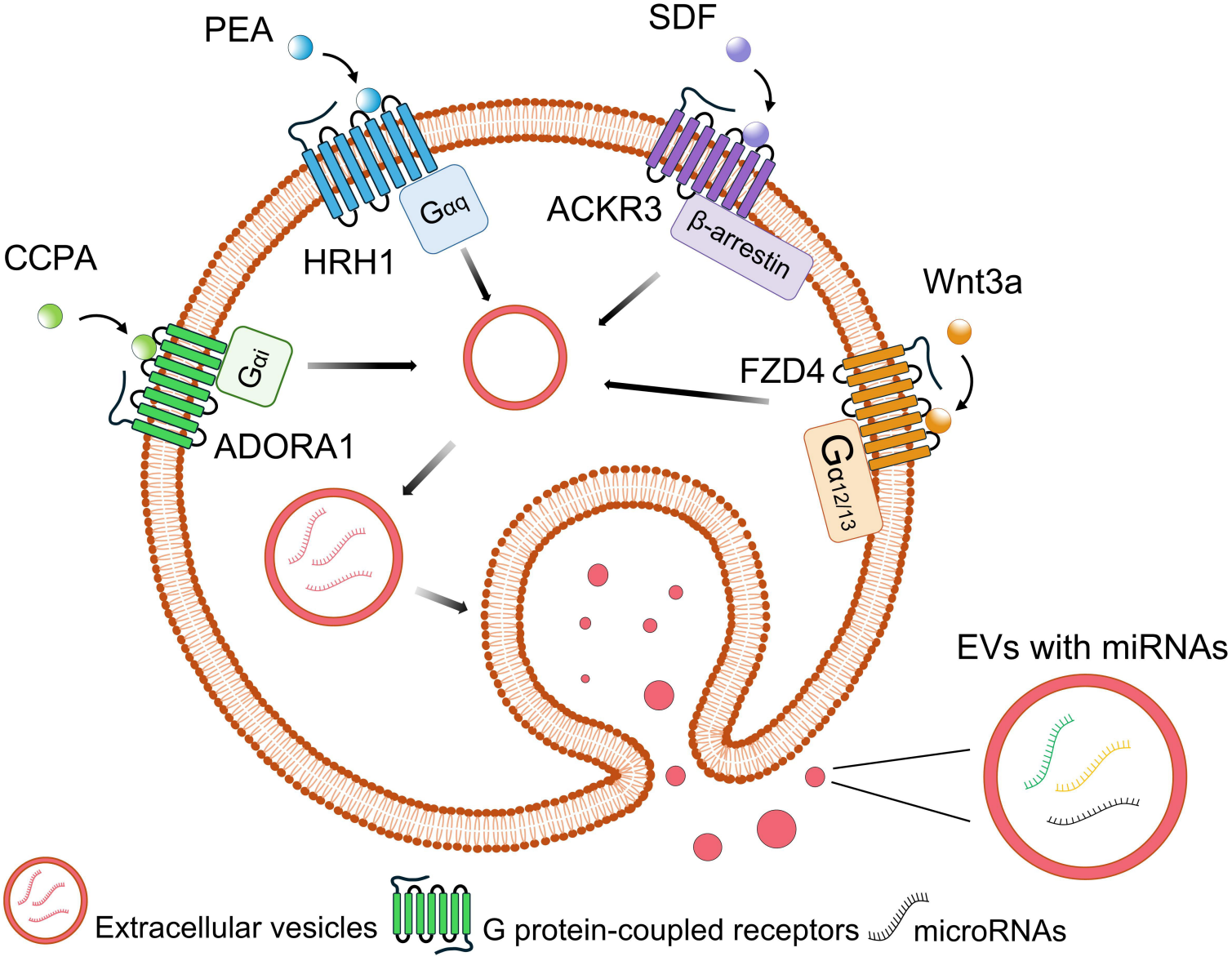
Stimulation of G protein-coupled receptors activates extracellular vesicle microRNA signatures